

<b>REPORT DOCUMENTATION PAGE</b>				<i>Form Approved</i> <b>OMB No. 0704-0188</b>	
Public reporting burden for this collection of information is estimated to average 1 hour per response, including the time for reviewing instructions, searching existing data sources, gathering and maintaining the data needed, and completing and reviewing this collection of information. Send comments regarding this burden estimate or any other aspect of this collection of information, including suggestions for reducing this burden to Department of Defense, Washington Headquarters Services, Directorate for Information Operations and Reports (0704-0188), 1215 Jefferson Davis Highway, Suite 1204, Arlington, VA 22202-4302. Respondents should be aware that notwithstanding any other provision of law, no person shall be subject to any penalty for failing to comply with a collection of information if it does not display a currently valid OMB control number. <b>PLEASE DO NOT RETURN YOUR FORM TO THE ABOVE ADDRESS.</b>					
<b>1. REPORT DATE (DD-MM-YYYY)</b>		<b>2. REPORT TYPE</b>		<b>3. DATES COVERED (From - To)</b>	
<b>4. TITLE AND SUBTITLE</b>				<b>5a. CONTRACT NUMBER</b>	
				<b>5b. GRANT NUMBER</b>	
				<b>5c. PROGRAM ELEMENT NUMBER</b>	
<b>6. AUTHOR(S)</b>				<b>5d. PROJECT NUMBER</b>	
				<b>5e. TASK NUMBER</b>	
				<b>5f. WORK UNIT NUMBER</b>	
<b>7. PERFORMING ORGANIZATION NAME(S) AND ADDRESS(ES)</b>				<b>8. PERFORMING ORGANIZATION REPORT NUMBER</b>	
<b>9. SPONSORING / MONITORING AGENCY NAME(S) AND ADDRESS(ES)</b>				<b>10. SPONSOR/MONITOR'S ACRONYM(S)</b>	
				<b>11. SPONSOR/MONITOR'S REPORT NUMBER(S)</b>	
<b>12. DISTRIBUTION / AVAILABILITY STATEMENT</b>					
<b>13. SUPPLEMENTARY NOTES</b>					
<b>14. ABSTRACT</b>					
<b>15. SUBJECT TERMS</b>					
<b>16. SECURITY CLASSIFICATION OF:</b>			<b>17. LIMITATION OF ABSTRACT</b>	<b>18. NUMBER OF PAGES</b>	<b>19a. NAME OF RESPONSIBLE PERSON</b>
<b>a. REPORT</b>	<b>b. ABSTRACT</b>	<b>c. THIS PAGE</b>			<b>19b. TELEPHONE NUMBER (include area code)</b>

# Final Report

## **S-layer architectures: Extending the morphogenetic potential of S-layer protein self assembly**

Agreement Award Nr.: FA9550-09-1-0342

Reporting period: May 1, 2009 to April 30, 2012

**Principal Investigator:** Dietmar Pum (PI) and Uwe B. Sleytr (Co-PI)

**Institution and address:** Department of Nanobiotechnology  
BOKU - University for Natural Resources and Life Sciences  
1190 Vienna, Austria

*Reporting date, 11 July 2012*

## Table of content

Executive Summary .....	4
List of publications .....	6
Statement of objectives .....	8
1 Introduction.....	9
2 Experimental work.....	11
2.1 Selection of S-layer proteins for this project.....	11
3 Liposomes.....	12
3.1 Recrystallization of S-layer proteins on liposomes .....	12
3.2 Silicification of plain liposomes and S-layer coated liposomes.....	12
3.3 Investigation of silica deposition on the nano-constructs.....	13
3.4 Characterization by Energy Filtered TEM (EFTEM) .....	15
3.5 Monitoring dissolution of the lipids by release experiments.....	18
3.6 Conclusions – Liposomes .....	20
3.7 Giant unilamellar vesicles – S-layer coating from the in-side .....	21
4 Emulsomes .....	23
5 Nanocapsules .....	24
5.1 S-layer coated calcium carbonate cores .....	24
5.2 Fluorescent S-layer fusion proteins .....	24
5.3 S-layer coated nanocapsules .....	26
5.4 Encapsulation of gold nanoparticles.....	28
5.5 Conclusion – Nanocapsules.....	29
6 Lipid lamellae, foams and microbubbles .....	30
6.1 S-layer protein – lipid lamellae .....	30
6.2 Conclusions – lipid lamellae and foams.....	32
6.3 S-layer coated microbubbles .....	33
7 Cylindrical S-layer morphologies (tubes).....	34
8 Design and expression of fluorescent S-layer fusion proteins and their spectroscopic characterization.....	35

8.1	Absorption, steady-state fluorescence, fluorescence lifetime and 2D self-assembly properties of engineered fluorescent S-Layer fusion proteins of <i>Geobacillus stearothermophilus</i> NRS 2004/3a.....	35
8.2	Fluorescent S-Layer Protein Colloids .....	36
8.3	Fluorescent energy transfer in the bi-fluorescent S-layer tandem fusionprotein ECFP-SgsE-YFP .....	36
9	Investigation of S-layer protein reassembly by electrochemical methods .....	37
9.1	Electrochemical control of adsorption dynamics of surface layer proteins on gold.....	37
9.2	Structural Control of Surface Layer Proteins at Electrified Interfaces investigated by In Situ Fourier Transform Infrared Spectroscopy.....	38
10	Molecular dynamic and Monte Carlo simulations of S-layer protein reassembly .....	38
10.1	Surface layer protein characterization by small angle x-ray scattering and a fractal mean force concept: From protein structure to nano-disc assemblies ...	39
10.2	Monte Carlo study of the molecular mechanisms of S-layer protein self-assembly .....	39
10.3	Atomistic structure of monomolecular surface layer self-assemblies: towards functionalized nanostructures .....	40
11	Single molecule force spectroscopy .....	41
11.1	Single-molecule force spectroscopy reveals the individual mechanical unfolding pathways of a surface layer protein .....	41
12	Conclusions from the project – Impact on the field .....	42
13	References .....	43

## Executive Summary

Nature has developed a broad range of nanometer scale architectures based on the self-assembly of molecular building blocks. An outstanding example has been optimized by nature during billions of years of evolution: *Crystalline bacterial surface layers, termed S-layers*. Based on the detailed knowledge about S-layer proteins the fabrication of three-dimensional hollow S-layer protein cages was defined as the main objective of this project. S-layers are the most commonly observed cell surface structures in prokaryotic organisms (bacteria and archaea). S-layers are highly porous protein meshworks with unit cell sizes in the range of 3 to 30 nm and pore sizes of 2 to 8 nm. One of the most remarkable and important properties for this project is their intrinsic tendency to reassemble into two-dimensional arrays in solution and at various interfaces.

S-layer coated liposomes have paved the way towards spatially expanded architectures. The mechanical robustness of S-layer coated liposomes was obtained by subsequent deposition of a thin layer of biogenic silica. Hollow S-layer protein cages were finally obtained after dissolution of the supporting liposomes with detergents. Proof-of-principle was shown by using liposomes previously filled with fluorescent dyes as scaffolds for S-layer reassembly and silica deposition and studying disruption and release of the dyes by fluorimetry. TEM and Electron Energy loss Spectroscopy (EELS) confirmed that hollow S-layer protein cages had been obtained.

In addition, 2-3  $\mu\text{m}$  sized nanocapsules with calcium carbonate ( $\text{CaCO}_3$ ) as core material were used as spherical scaffolds, too. The particles could be downsized to a few hundred nanometers. The particles were fluorescently labeled, coated with S-layer protein and silicified. Dissolution of the core lead to stable silica supported S-layer architectures as demonstrated by fluorescence microscopy and SEM. According to the project plan this approach was repeated with the addition of coating the core material with polyelectrolyte layers prior to the S-layer reassembly. Again, as shown for nanocapsules without polyelectrolyte coating a complete dissolution of  $\text{CaCO}_3$  was possible, too. The remaining,

hollow nanocapsules composed of polyelectrolytes and S-layer were mechanically stable and could be well characterized by TEM, AFM and SEM.

The reassembly of S-layer protein on gas filled micro bubbles and at foam lamellae was investigated, too. This work is the basis for the reassembly of S-layer proteins in foams and the making of 3D-polyhedral architectures.

Making 3D-structure predictions of the S-layer protein supported the experimental work. Further on, Monte-Carlo simulations were used to investigate the self-assembly process. A most remarkable result was obtained by single molecule force spectroscopy where it was found that the interaction of the S-layer protein with the secondary cell wall polymer of the associated bacterial cell wall increases the strength of the S-layer protein.

It is anticipated that three-dimensional S-layer architectures may be used for a broad range of novel applications ranging from the development of artificial viruses, controlled drug targeting and delivery to spatially constrained synthesis of nanoparticles.

Part of the work is published already in high-impact journals (11 SCI indexed publ.).

## List of publications 2009 – 2012

1. Zafiu, C., Trettenhahn, G., Pum, D., Sleytr, U.B., Kautek, W. 2011. Structural Control of Surface Layer Proteins at Electrified Interfaces investigated by In Situ Fourier Transform Infrared Spectroscopy. *Phys. Chem. Chem. Phys.* 13:13232-13237
2. Horejs, C., Ristl, R., Tscheliessnig, R., Sleytr, U.B., Pum, D. 2011. Single-molecule force spectroscopy reveals the individual mechanical unfolding pathways of a surface layer protein. *J. Biol. Chem.* 286:27416-27424
3. Horejs, C., Gollner, H., Pum, D., Sleytr, U.B., Peterlik, H., Jungbauer, A., Tschliessnig, R. 2011. Atomistic structure of monomolecular surface layer self-assemblies: towards functionalized nanostructures. *ACS Nano* 5:2288-2297
4. Zafiu, C., Trettenhahn, G., Pum, D., Sleytr, U.B., Kautek, W., 2011. Electrochemical control of adsorption dynamics of surface layer proteins on gold. *Phys. Chem. Chem. Phys.* 13:3478-3483
5. Horejs, C., Mitra, M. K., Pum, D., Sleytr, U.B., Muthukumar, M. 2011. Monte Carlo study of the molecular mechanisms of S-layer protein self-assembly. *J. Chem. Phys.* 134: 125103-1 – 125103-11
6. Horejs, C., Pum, D., Sleytr, U.B., Peterlik, H., Jungbauer, A., Tscheliessnig, R. 2010. Surface layer protein characterization by small angle x-ray scattering and a fractal mean force concept: From protein structure to nano-disc assemblies. *J. Chem. Phys.* 133:175102-1-175102-8
7. Kainz, B., Steiner, K., Sleytr, U.B., Pum, D., Toca-Herrera, J. L. 2010. Fluorescent energy transfer in the bi-fluorescent S-layer tandem fusionprotein ECFP-SgsE-YFP. *J. Struct. Biol.* 172:276-283
8. Kainz, B., Steiner, K., Sleytr, U.B., Pum, D., Toca-Herrera, J. L. 2010. Fluorescent S-Layer Protein Colloids. *Soft Matter* 6:3809-3814
9. Kainz, B., Steiner, K., Möller, M., Pum, D., Schäffer, C., Sleytr, U.B., Toca-Herrera, J.L. 2010. Absorption, steady-state fluorescence, fluorescence lifetime and 2D self-assembly properties of engineered fluorescent S-Layer fusion proteins of *Geobacillus stearothermophilus* NRS 2004/3a. *Biomacromolecules*, 11:207-214
10. Göbel, C., Schuster, B., Baurecht, D., Sleytr, U.B., Pum, D. 2009. S-layer templated bioinspired synthesis of silica. *Coll. Surf. B: Biointerfaces*, 75:565-572
11. Badelt-Lichtblau, H., Kainz, B., Völlenkle, C., Egelseer, E.M., Sleytr, U.B., Pum, D., Ilk, N. 2009. Genetic engineering of the S-layer protein SbpA of *Lysinibacillus sphaericus* CCM 2177 for the generation of functionalized nanoarrays. *Bioconjugate Chem.* 20:895-903

## Mansucripts in preparation / submitted

1. Pum, D., Schuster, D., Küpcü, S., Belton, D. J., Perry, C. C., Stöger-Pollach, M., Sleytr, U.B., Construction of silica enhanced S-layer protein cages, *Acta Biomaterialia* (submitted)

2. Schuster, D., Kainz, B., Sleytr, U.B., Pum, D., Fabrication of robust hollow nanocapsules (in prep.)
3. Pum, D., Schödelbauer, M., Sleytr, U.B., Toca-Herrera, J. L., Biophysical properties of S-layer protein / surfactant foam lamellae and monolayers (in prep.)

### **Book chapters**

1. Sleytr, U.B., Schuster, B., Egelseer, E.M., Pum, D., Horejs, C.M., Tscheliessnig, R., Ilk, N. 2011. Nanotechnology with S-Layer Proteins as Building Blocks pp.277-352. In: Horwoka, S. (Ed.), Progress in Molecular Biology and Translational Science 103, Academic Press, Burlington, MA (USA).
2. Pum, D., Tang, J., Hinterdorfer, P., Toca-Herrera, J. L., Sleytr, U.B. 2010. S-layer protein lattices studied by scanning force microscopy. p.459-510. In: Kumar, C. (Ed.), Biomimetic and bioinspired nanomaterials, Vol. 7., Wiley-VCH, Weinheim, Germany.

### **PhD Thesis**

1. Christine Horejs, The structure and assembly of surface layer proteins: a combined approach of in silico and experimental methods. Universität für Bodenkultur Wien (2011)
2. Birgit Kainz, Fluorescent S-layer fusion proteins. Universität für Bodenkultur Wien (2010)

### **Master thesis**

1. Michael Schödelbauer. Biophysical properties of S-layer protein / surfactant foam lamellae and monolayers. Universität für Bodenkultur Wien (2012)



## Statement of objectives

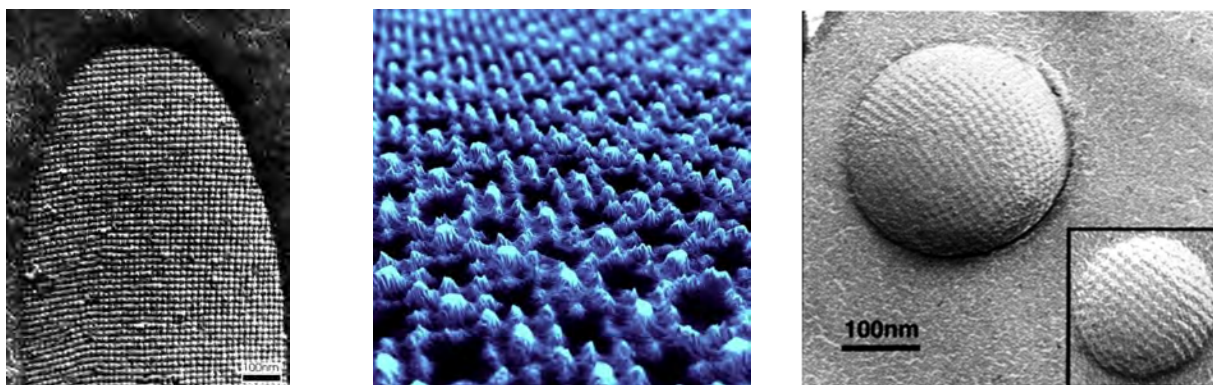
The main objective of the proposed work was the fabrication of three-dimensional S-layer protein architectures. Micrometer sized hollow morphologies were created. Surface engineering with polyelectrolyte layers allowed us to functionalize the architectures using simple liquid handling procedures. It is anticipated that three-dimensional S-layer architectures will be used for a broad range of novel applications ranging from the development of artificial viruses, controlled drug targeting and delivery (including hydrophobic substances), affinity matrices, medical applications, stable foam like structures, to spatially constrained synthesis of nanoparticles.

The following objectives were defined in order to meet the goal of this project.

Objective	Status at end-of-project
Generation of spherical S-layer cages	completed
Generation of polyhedral S-layer morphologies	Work with foam lamella completed, with foam bubbles in progress
Generation of cylindrical S-layer morphologies	Work with carbon nanotubes in progress
Functionalization of S-layer architectures	completed
Characterization of the S-layer architectures	completed
Exploitation and dissemination of the results	part of the work already published (11 SCI publications), further manuscripts submitted or in preparation

## 1 Introduction

Nature has developed a broad range of nanometer scale architectures based on the self-assembly of molecular building blocks. While some of this nanometer scale three-dimensional structures are artistically and ambitiously shaped morphologies, like the well known silica frustules of diatoms <sup>1</sup> and silica spicules of mineralized sponges <sup>2</sup>, others impress by their simple geometrical shape. Prime candidates of the latter group are the protein shells of viruses (called capsids) exhibiting either helical or icosahedral structure. <sup>3</sup> <sup>4</sup> The helical shape is cylindrical but the icosahedral one, which consists of 20 equilateral triangular faces, approximates a sphere. Although bottom-up based building principles are well understood and the building blocks often fully characterized, only a few man-made biological architectures have been introduced into the scientific community so far. An example is the cavity of the cage-shaped protein apoferritin used for the synthesis of iron nanoparticles. <sup>5,6</sup> Another example which has been optimized by nature during billions of years of evolution are *crystalline bacterial surface layers*, termed S-layers. <sup>7-9</sup> S-layers are the most commonly observed cell surface structures in prokaryotic organisms and are found in a broad range of bacteria and archaea (Fig.1a). S-layers fulfill various functions for the bacterial or archaeal cell such as providing molecular sieving characteristics in the ultrafiltration range <sup>10</sup> or acting as rigid corset in the shape determination of various archaeal cells. <sup>11,12</sup> One of the most remarkable properties of S-layer proteins is their intrinsic tendency to form two-dimensional arrays in solution <sup>13</sup>, at solid supports (Fig.1b) <sup>14,15</sup>, at the air-water interface <sup>16,17</sup>, on planar lipid films <sup>18</sup>, at liposomes <sup>19-21</sup> (Fig.1c) and nanocapsules <sup>22-24</sup>. Although S-layer proteins reassemble only in plane (in mono- or double layers), the coating of liposomes with S-layer proteins has demonstrated that closed three-dimensional protein containers may be fabricated *in vitro*, too (Fig.1c). Due to the introduction of lattice faults, such as disclinations that are a necessity for two-dimensional crystals to cover curved surfaces, the rigidity and isoporosity of the entire S-layer meshwork is maintained. <sup>11,12</sup>



(a)

(b)

(c)

Fig.1 (a) TEM image of a freeze-etched and metal shadowed preparation of a bacterial cell exhibiting an S-layer with square (p4) lattice symmetry. (b) Perspective view of an S-layer protein monolayer recrystallized on a silicon surface. The size of the unit cell is 13.1 x 13.1 nm. Image data were obtained by AFM and processed by computer graphics methods. (c) TEM image of a freeze-etched and metal shadowed preparation of S-layer coated liposomes.

The main objective of the proposed work was the fabrication of three-dimensional S-layer protein architectures and was derived from our know-how to make S-layer coated liposomes.<sup>19-21</sup> Thus, the main focus of our work was dedicated to mechanically stabilize the surface of S-layer coated liposomes and subsequently to remove the lipid content of the nanoporous constructs. The mechanical robustness of S-layer coated liposomes was obtained by deposition of a thin layer of biogenic silica (Figure 2).<sup>25</sup> But liposomes were not the only model system used in this project: Nanocapsules (with micron sized calcium carbonate cores) and functionalized by a layer-by-layer deposition of polyelectrolytes and subsequent S-layer coating were investigated, too.<sup>22-24</sup> In addition to the spherical architectures, preliminary work on polyhedral morphologies, such as foam bubbles, was performed. For this purpose, the film thinning in S-layer supported foam lamella was investigated in detail while in another approach the reassembly of S-layer protein at micron sized gas filled bubbles in water yielded first results for the making of unsupported S-layer cages. The experimental work was supported by calculating 3D-structure predictions of the S-layer proteins<sup>26,27</sup> and by investigating their self-assembly process by Monte-Carlo simulations.<sup>28</sup> A most remarkable result was obtained by single molecule force spectroscopy where it was found that the interaction of the S-layer protein with the secondary cell wall polymer of the associated bacterial cell wall increases the strength of

the S-layer protein.<sup>29,30</sup> The following chapters provide a detailed description of the work done.

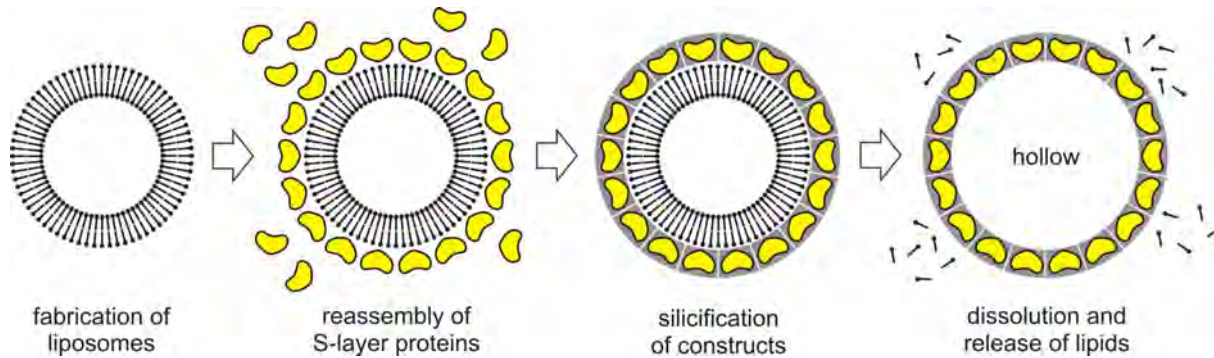


Fig.2 Schematic drawing of the consecutive preparation steps for making hollow silica enhanced S-layer cages.

## 2 Experimental work

### 2.1 Selection of S-layer proteins for this project

From preliminary studies and current work we decided to work with the following S-layer proteins:

- SbsB from *Geobacillus stearothermophilus* PV72/p2 (oblique (p1) lattice symmetry;  $a=10.4$  nm,  $b=7.9$  nm,  $\gamma=81^\circ$ ,  $d=4.5$ nm),<sup>31</sup> and
- SbpA from *Lysinibacillus sphaericus* CCM2177 (square (p4) lattice symmetry;  $a=13.1$ nm,  $d=9$ nm).<sup>32</sup>
- SgsE from *Bacillus stearothermophilus* NRS2004/3a (oblique (p2) lattice symmetry;  $a=9.4$ nm,  $b=11.6$ nm,  $\gamma=78^\circ$ ,  $d=5$ nm)<sup>33</sup>

In addition, several recombinant S-layer fusion proteins have already been developed, too.

<sup>34-36</sup> While a 3D-structure prediction was available for SbsB already,<sup>26</sup> a prediction for

SbpA was completed in the course of this project.<sup>27</sup> Both models are published already. The elucidation of the 3D-Structure of SgsE is currently under investigation.

### 3 Liposomes

#### 3.1 Recrystallization of S-layer proteins on liposomes

Based on previous work the S-layer protein SbsB from *Geobacillus stearothermophilus* PV72/p2 was reassembled on unilamellar liposomes with mean diameters of 130 nm.<sup>19-21</sup> The size distribution of the liposomes and the successful reassembly of the proteins were determined by TEM. Plain (uncoated) and S-layer coated liposomes were negatively stained after adsorption on carbon coated electron microscopy grids. Figure 3 shows examples of (a) plain and (b) S-layer coated liposomes. The S-layer protein reassembles into contiguous mono-crystalline patches on the surface clearly separated by line defects. These lattice faults may either originate from wedge-disclinations which are a necessity for the two-dimensional layer to cope with the curvature or simply as a consequence of the independently initiated and subsequently growing crystalline domains on the liposome surface.

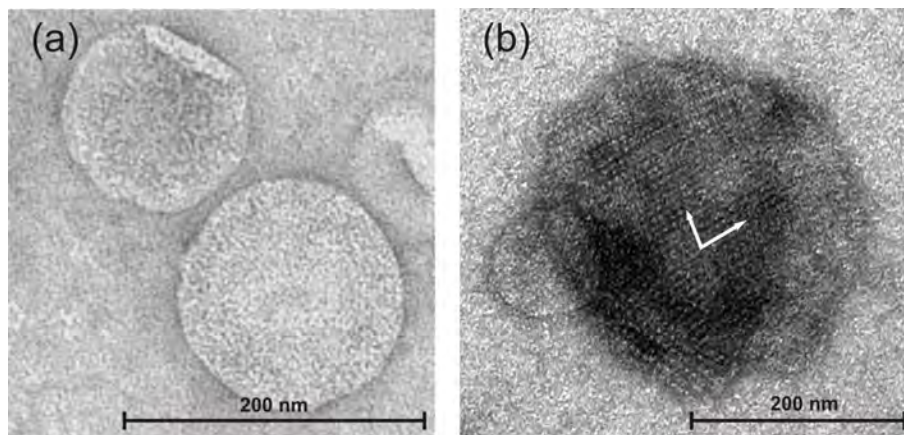


Fig.3 TEM micrographs of negatively stained (a) plain (uncoated), and (b) rSbsB coated liposomes. The base vectors indicate the oblique (p1) lattice symmetry

#### 3.2 Silicification of plain liposomes and S-layer coated liposomes

Plain and S-layer coated liposomes were silicified,<sup>25</sup> washed and investigated in the TEM without further negative staining, e.g. with uranyl acetate. Thus the contrast in TEM images



originates from deposited silica (Figure 4). Since silica is not a high resolution staining material, structural details like the S-layer pattern cannot be seen. Energy dispersive X-ray analysis (EDX) confirmed the presence of silica on both plain and S-layer coated liposomes (Figure 4).

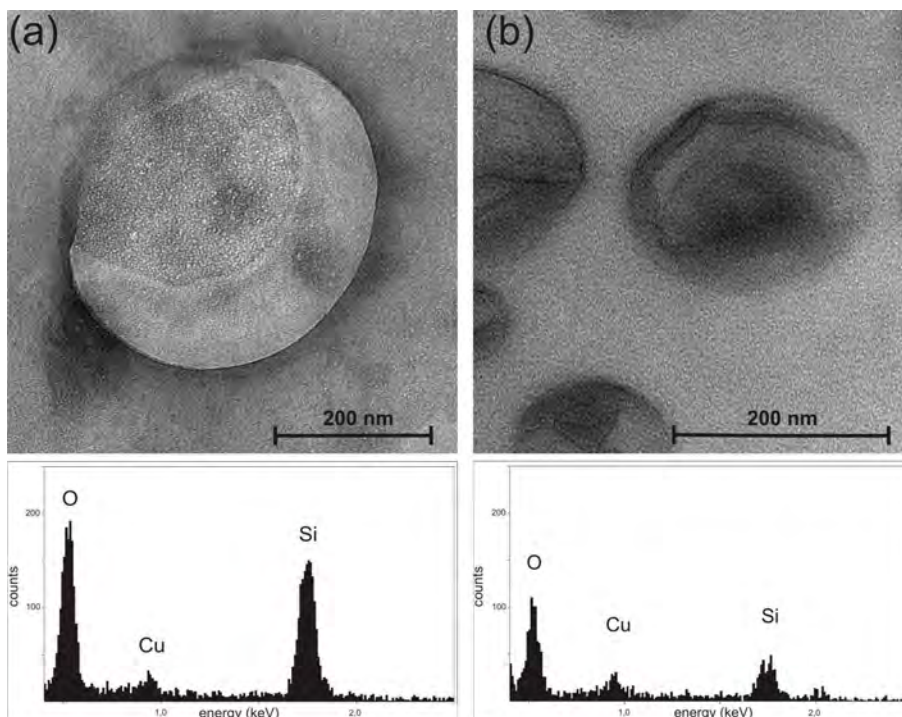


Fig.4 Confirmation of the presence of a silica layer on plain and S-layer coated liposomes using TEM with EDX analysis (60 min silica condensation time). The samples were not negatively stained, the contrast originates from silica. (a) Plain and (b) rSbsB coated silicified liposomes. The corresponding EDX spectra showing the Si-peaks are placed beneath the TEM images.

### 3.3 Investigation of silica deposition on the nano-constructs

A detailed characterization of the silica deposition process, in particular on the influence of the silicification time on the  $\zeta$ -potential of the constructs was performed (Figure 5). The condensation reaction was stopped after defined time intervals and the  $\zeta$ -potential of the particle suspension measured while titrating from pH 4 to pH 8.

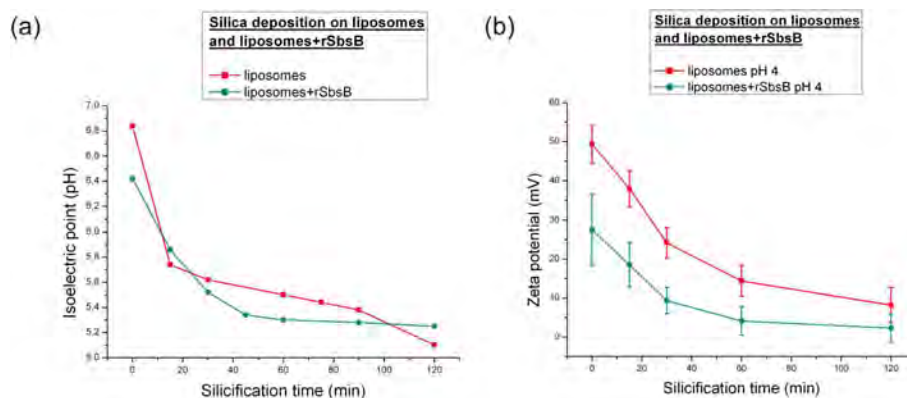


Fig.5  $\zeta$ -potential measurements of plain and S-layer coated liposomes subjected in relation to time of silicification. (a) isoelectric points and (b)  $\zeta$ -potential shift of silicified plain and S-layer coated liposomes.

The background contribution of silica deposition was measured without liposomes in the condensing system (data not shown). The  $\zeta$ -potential of the background was found to vary only slightly with pH and silicification time. Thus, it was concluded that the silica background does not have great impact on the  $\zeta$ -potential of the silicified constructs. Determination of the isoelectric point for the samples ( $\zeta$ -potential is zero for a specific pH value) yielded almost no significant differences between the plain and S-layer coated liposomes (Figure 5 (a)). Further evidence for the formation of silica on the surface of the liposomes was found from the time dependent decrease of the isoelectric point due to the more negative (surface) charge of silica.

With increasing silicification (condensation) time the shifts of the measured  $\zeta$ -potentials were much more pronounced for plain liposomes compared to S-layer coated liposomes (Figure 5 (b)). In addition, after 60 min silica condensation the  $\zeta$ -potential of S-layer coated liposomes approached a constant value of about 5 mV. This can be explained by a charge shielding effect compensating the charge of the S-layer proteins leading to smaller changes of the  $\zeta$ -potential in the course of the reaction.

In addition to the silicification of plain and S-layer coated liposomes, silica deposition was investigated on rSbsB monolayers reassembled on carbon coated EM-Grids, too. The experiments were carried out at pH 5, 7 and 9. The relative amount of silica was estimated by EDX analysis in the TEM. The highest silica deposition was found at pH 7 in accordance with what would be expected.

### 3.4 Characterization by Energy Filtered TEM (EFTEM)

A TEM equipped with an imaging Electron Energy Loss Spectrometer (EELS) was used to investigate the distribution, the electronic structure and the thickness of the deposited silica layers. This technique is also referred to as Energy Filtered TEM (EFTEM). Thin sections of plain and S-layer coated silicified liposomes were prepared. EFTEM data show silica deposition on plain liposomes as a bright layer along its surface. Since biological material, such as the lipid bilayer of the liposomes or the reassembled S-layer cannot be seen in EFTEM silica maps, conventional bright field TEM was used to image the same sample area for comparison. Silicified plain liposomes tend to aggregate which complicates a reliable thickness determination of the silica layer on single liposomes. However, the thickness of the silica layer was in the range of 3.5 and 7nm but was unevenly distributed (Figure 6). This effect can be explained by the fact that depending on the thickness and orientation of the cross sectioned liposome membrane, different images are generated in the 2D projection.

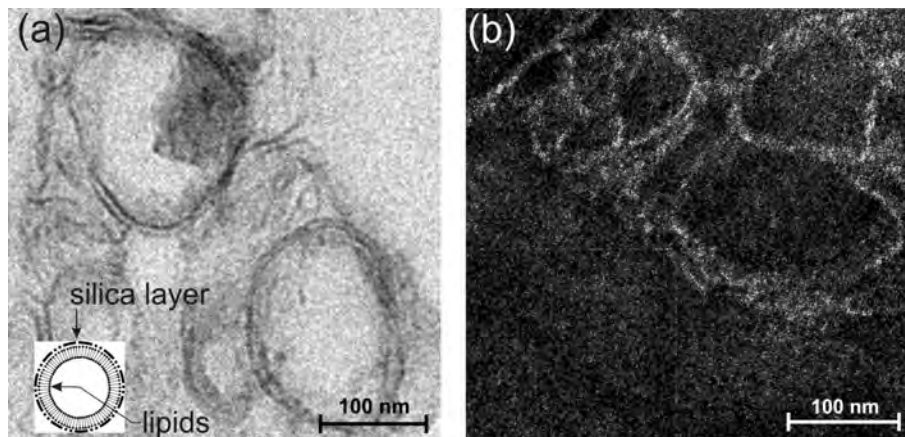


Fig.6 Ultra thin sections of plain liposomes (silicified for 120 min) visualized by (a) TEM (Insert showing the schematic drawing of the constructs) and (b) silica distribution in a specimen visualized by EFTEM.

In contrast to plain liposomes, S-layer coated liposomes scarcely aggregated. As shown in Figure 7, some of the liposomes collapse. The S-layers appear as weak electron scattering, diffuse structures along with the more electron dense lipids. The particles are separate and so the thickness of the silica layer can be reliably measured and correlated to the



silicification time. The respective thicknesses were 2.5 nm, 6 nm and 7 nm for 30, 60 and 120 min silica deposition times, respectively. This indicates that the thickness of the silica layer did not increase linearly with time. The reaction was almost completed after 60 minutes.

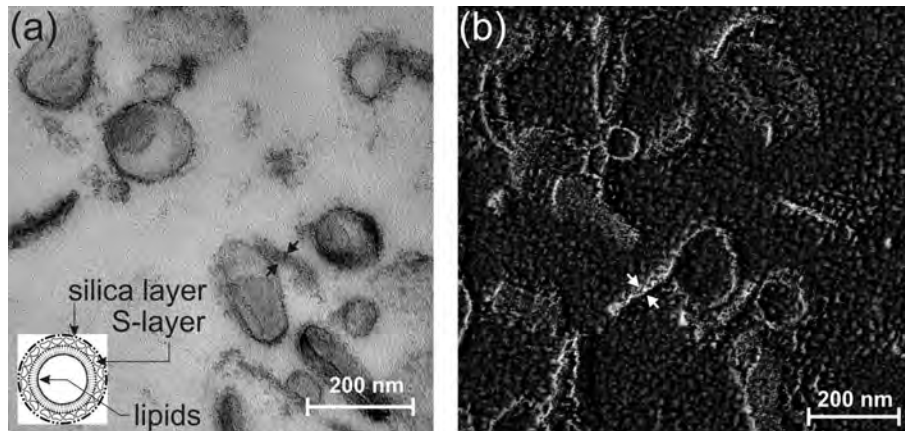


Fig. 7 Ultra thin sections of S-layer coated liposomes silicified for 120 minutes visualized by (a) TEM (Insert showing the schematic drawing of the constructs) and (b) silica distribution in a specimen analyzed by EFTEM. Arrows show silicified S-layer monolayers.

Since silicification times of 60 and 120 min showed similar silica layer thicknesses, 60 min was chosen for the construction of silica- and silica supported S-layer cages in the experiments described below. These constructs were used in the following to obtain hollow structures after removal of the scaffolding lipids. Mild conditions were mandatory to avoid destruction of the silica constructs and the proteins, respectively. As shown previously,<sup>20</sup> extraction of the lipid bilayer with Triton X-100 was appropriate. TEM analysis was used to explore the effect of detergent treatment on the stability of the cages. Images of ultra thin sectioned plain silica cages showed coalescing liposome fragments (Figure 8 (a)). As such a phenomenon is not observed for silicified liposomes before detergent treatment, we assume that together with the extracted lipids also weakly silicified bridging lipid lamellae were removed. It was concluded that liposomes aggregate in an early stage of the silica condensation process and thus these lipid lamellae were not accessible for silicification. EELS maps indicate an inhomogeneous silica distribution with layer thicknesses of up to 11 nm (Figure 8 (b)). The energy loss near edge structure (ELNES) of the Si edge, which reflects the electronic structure of the probed Si atoms, confirms the presence of oxidized

silicon on the particle surface (data not shown). Potential interaction of the silica with remnants of lipids could not be detected with this method.

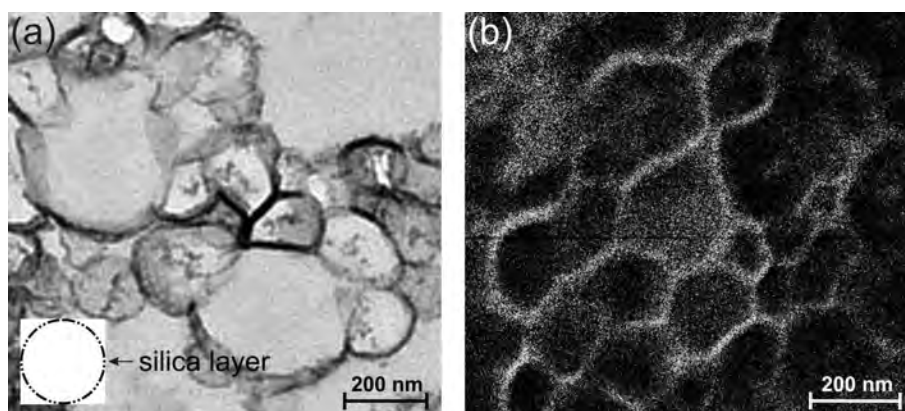


Fig.8 Ultra thin sections of plain liposomes (silicified for 60 minutes) after lipid extraction with TRITON X-100, visualized by (a) TEM (Insert showing the schematic drawing of the constructs) and (b) silica distribution in a specimen visualized by EFTEM.

Silicified S-layer coated liposomes, extracted with Triton X-100, show well separated, silicified S-layer constructs (Figure 9). The thickness of the silica layer is about 6 nm. Although no mechanical studies of these constructs have been performed, the fact that the structural integrity of the particles was maintained indicates that the silica coating stabilizes the architecture.

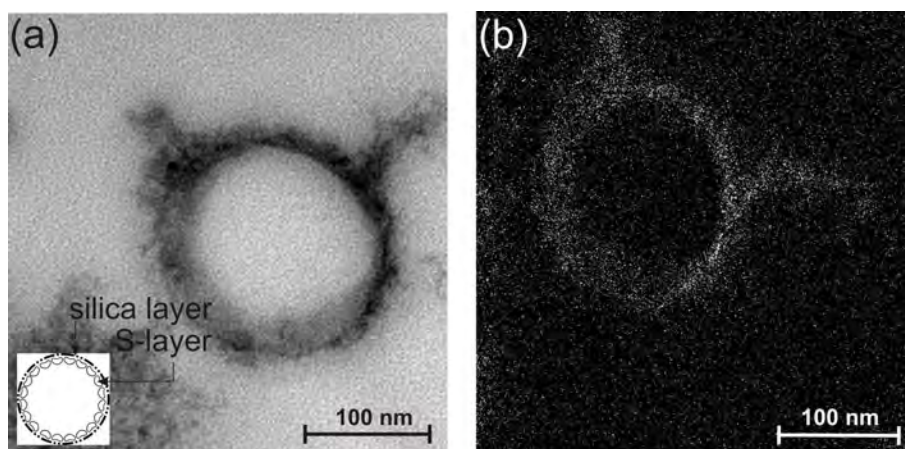


Fig. 9 Ultra thin sections of S-layer coated liposomes (silicified for 60 minutes) after lipid extraction, visualized by (a) TEM (Insert showing the schematic drawing of the constructs) and (b) silica distribution in a specimen visualized by EFTEM.

It must be noted that the silicified liposomes show aggregation whereas the S-layer coated liposomes remain separated. In addition, silica deposition gives enough contrast in bright field TEM to visualize adsorbed plain and S-layer coated liposomes (in top on view) but only highly sensitive EELS mapping allowed a quantification of the thickness of the thin silica layer.

### 3.5 Monitoring dissolution of the lipids by release experiments

In order to monitor the dissolution of the lipid scaffold, a fluorescent dye (5-(6)-carboxyfluoresceine (CF)) was enclosed in the liposomes during preparation. Due to the tight packing of the dye in the interior of the liposomes its fluorescence is self quenching but upon dissolution of the lipid shell and release of the dye molecules, the fluorescence immediately rises.<sup>40</sup> CF encapsulated in liposomes and S-layer coated liposomes was released after addition of Triton X-100 which provides evidence for the dissolution of the scaffolding lipid structures (see

Table 1). To check if the added amount of detergent was sufficient to disrupt the lipid membranes and to release the encapsulated CF, the concentration of Triton X-100 was raised from 0.5 % to 1.0 % . Since the fluorescent signal did not increase, it was concluded that the concentration of 0.5 % was sufficient for total release. Detergent and fluorescent dyes penetrate the silica or the protein/silica layer, respectively, by passive transport in both directions.

**Table 1.** Release of carboxyfluoresceine (induced by treatment with Triton X-100) from plain liposomes (CFL) and S-layer coated liposomes (S-CFL) in relation to increasing silicification times.

Release R [%]	CFL	CFL 0 min Si	CFL 30 min Si	CFL 60 min Si	CFL 120 min Si
	64+/-2	21+/-2	28+/-0	28+/-1	28+/-0
	S-CFL	S-CFL 0 min Si	S-CFL 30 min Si	S-CFL 60 min Si	S-CFL 120 min Si
	82+/-7	58+/-2	83+/-2	78+/-4	77+/-2

The relative amount of released dye was calculated as the difference of the spectroscopic signal before and after silicification (and treatment with Triton X-100) using the formula:  $R = (f_a - f_b) / f_a \cdot 100$  ( $R$  is the amount of released CF in %,  $f_b$  and  $f_a$  are the fluorescence before and after addition of Triton X-100). Addition of the silica precursor and immediate stopping of the reaction with hydrochloric acid (0 min Si in Table 1) yielded a release of 21% and 58%. Since this result was surprisingly low a blank silicification reaction in the presence of CF in solution was carried out. The silicification had no influence on the fluorescent signal and thus a mutual interaction was excluded. Thus, it was assumed that the low release rates at 0 min may be outliers due to inhomogeneities of the reaction mix in the startup phase or may indicate a non-uniform release behavior of different populations of liposomes. It is well known that S-layer coated liposomes are more stable than plain liposomes.<sup>20,41</sup> This explains the higher release values for S-CFLs. The release seems to be independent of the silicification time, as no significant differences were found between 30, 60 and 120 min of silicification time. The silica layer appears to be porous since the detergent Triton X-100 on the one hand and lipids and CF on the other hand can penetrate it. This indicates that the lipids in the fabricated structures can at least be disrupted and partly dissolved to trigger a release of CF. We could not find a causal correlation between the release kinetics of CF out of the plain and S-layer coated liposomes with different silicification times (Figure 10). The release kinetics is faster for S-CFL than for plain CFLs. CFLs exhibit a broader distribution in the release curves, whereas S-CFLs show a well defined homogenous release through

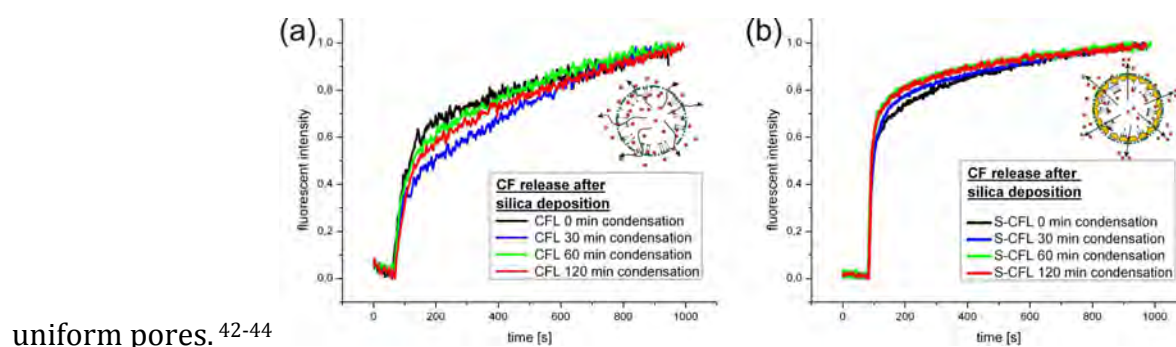


Fig.10 Time resolved release of CF from (a) plain and (b) S-layer coated liposomes after various silicification times.

Probably only a certain amount of liposomes, without uniform release behavior, are dissolved within the observed time frame. This means that for a complete dissolution of the lipid membranes with Triton X-100 at room temperature, a measurement time of 1000

seconds is too short. As described by Sila et al. , Triton X-100 concentrations as low as 0,5 % will only efficiently disrupt unilamellar liposomes. Since further addition of Triton X-100 to 1 % total concentration did not lead to an increase in the fluorescent signal, most of the liposomes are unilamellar as we expected due to the extrusion process. Despite the long incubation with Triton X-100 during dialysis, it is not likely that all lipids were extracted from the silica- or silica supported S-layer cages. Further experiments need to be done to elucidate whether the remaining lipids still have a major contribution to the integrity of the constructs. These experiments confirm a partly dissolution of the lipid structures such that most of the entrapped CF is released.

### 3.6 Conclusions – Liposomes

Plain and S-layer coated liposomes were successfully silicified. Silica was visualized, elemental analysis confirmed the presence of Si and the layer thickness of the silica layer was determined. After removal of the lipids used to generate the liposome scaffolds, stable hollow S-layer protein cages were obtained. Disruption of the lipid bilayer was monitored by fluorescent release of silicified and carboxyfluoresceine filled plain and S-layer coated liposomes. Detergent Triton X-100 and fluorescent dye could penetrate the silica layer and the silicified S-layer, respectively. Different release behavior was found for the plain and S-layer coated silicified liposomes. Silicification had an influence on the surface charge of the constructs. Such measurements allow to monitor the extent of the silica deposition.

It is anticipated that our approach to make hollow, stable S-layer cages will allow the development of novel encapsulation techniques, for example in nano medicine, but also for the construction of new materials with special physicochemical properties such as photonic crystals. and represents another tool in the development of a molecular construction kit.

#### **Manuscript:**

#### **Construction of silica supported S-layer coated liposomes**

Schuster, D., Küpcü, S., Belton, D.J., Perry, C.C., Stöger-Pollach, M., Sleytr, U.B., Pum, D., Acta Biomaterialia (submitted)

**Note:** This work was performed in close collaboration with Prof. Carole C. Perry, Nottingham Trent University, UK.

### 3.7 Giant unilamellar vesicles – S-layer coating from the in-side

Based on the work with liposomes, it was anticipated that it should be possible to make liposomes having an S-layer protein layer at the inner and an (optionally different) S-layer coating on the outer surface. In this way a new highly anisotropic spherical architecture would become possible. A silica layer could stabilize the construct from the inner face, too. Since, for complete coverage of the inner surface, rather large volumes of protein solution need to be encapsulated giant unilamellar vesicles (GUVs) were used. For example, assuming  $6 \text{ mg} \cdot \text{ml}^{-1}$  as maximum solubility of SbsB, liposomes at least  $2 \text{ }\mu\text{m}$  in diameter are needed in order to encapsulate the required volume of protein solution.

The preparation of the GUVs followed standard preparation techniques (molar ratio DPPC:Chol:HDA = 10:5:4; 0,02% Bodipy). Fluorescence microscopy was used to control and characterize size, shape and integrity of the GUVs (Figure 11).

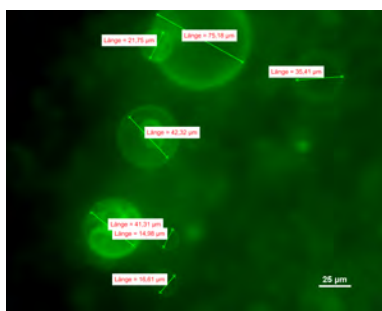


Fig.11 Fluorescence microscopy image of GUVs used in this project.

A set of structures was prepared (see Figure 12):

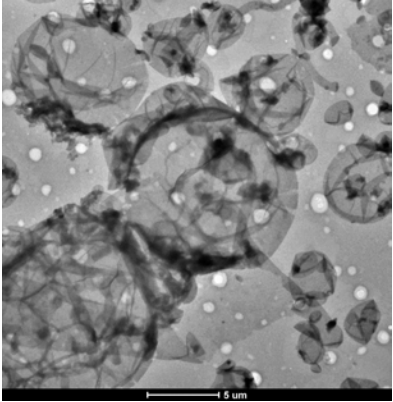
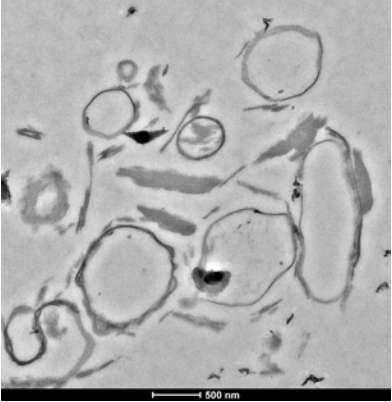


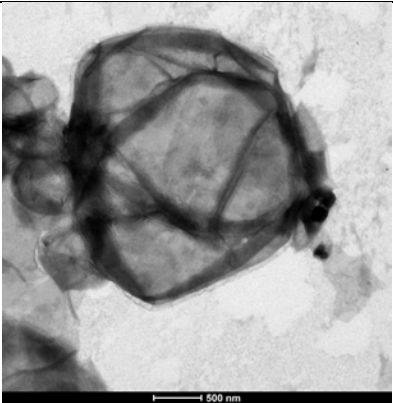

	TEM negatively stained preparation	TEM ultra thin section
outer face coated with S-layer		
outer and inner face coated with S-layers		
inner face coated with S-layer		

Fig.12 TEM micrographs of negatively stained preparations and ultrathin section of S-layer coated GUVs.

In the first set of experiments S-layer protein SbsB was reassembled on the outer surface of the GUVs (Figure 12 top row). In the following sets, for the reassembly of the S-layer



protein from the in-side SbsB was immersed into the lipid solution prior to GUV formation. TEM of ultrathin sections demonstrated that - as a preliminary result – SbsB reassembles at the inner and at the outer surface of the GUVs (Fig.12 middle and bottom row). Finally, the outer S-layer was removed by the chaotropic agent GHCl in a concentration of 4 M while the inner S-layer remains intact due to the protective lipid bilayer of the GUVs (Fig.12 bottom row), This was demonstrated by TEM of ultra thin sections in combination with QCM-D studies (Fig.13): After the adsorption of GUVs onto the sensing surface S-layer protein was reassembled at the outer surface and subsequently removed again by treatment with GHCL. Thus the S-layer seen in TEM images of negatively stained preparations must be the inner S-layer.

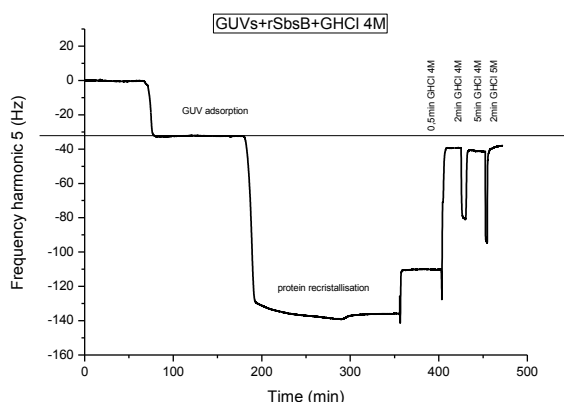


Fig.13 QCMD-data showing the adsorption of GUVs followed by the reassembly of S-layer protein at the outer surface. Subsequently the outer S-layer was removed by GHCL again.

## 4 Emulsomes

Emulsomes were used as a proof-of-concept (Figure 14). Their core of pure lipids was much harder to dissolve and complicated the extraction in order to get pure S-layer cages. Therefore no more effort was put into it.



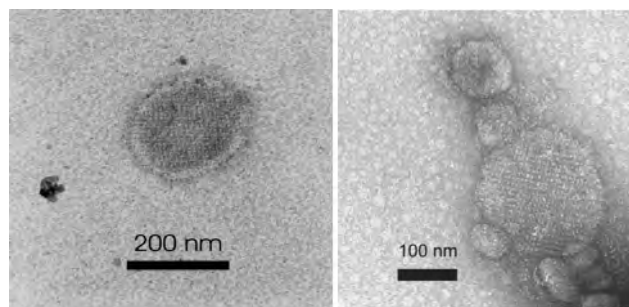


Fig. 14 TEM images of negatively stained preparations of S-layer coated emulsomes.

## 5 Nanocapsules

### 5.1 S-layer coated calcium carbonate cores

Apart from liposomes, differently sized calcium carbonate ( $\text{CaCO}_3$ ) particles (mean diameter, 1-5  $\mu\text{m}$ ) were used as scaffolds for making S-layer cages, too. The particles were fabricated using standard procedures. Figure 15 shows an SEM image of such cores.

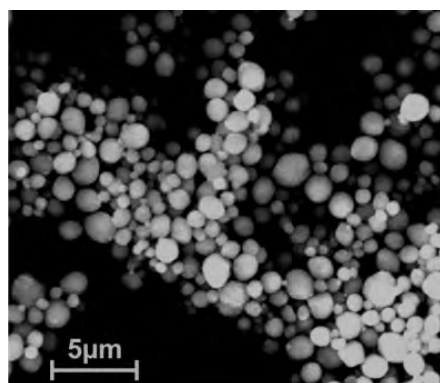


Fig.15 SEM image of calcium carbonate ( $\text{CaCO}_3$ ) particles with a mean diameter of  $1.0 \pm 0.3 \mu\text{m}$ .

### 5.2 Fluorescent S-layer fusion proteins

Several S-layer fusion proteins were designed and expressed in the course of this project. The fusion proteins SgsE-mRFP and SgSE-EGFP fusion proteins combine the self assembly properties of the S-layer protein SgsE from *Geobacillus stearothermophilus* NRS 2004/3a with the fluorescence of the monomeric red or green fluorescent proteins. The spectroscopic characterization and additional applications are published already (summarized later in this report). The use of fluorescent S-layer fusion proteins made it

much easier to investigate the formation of S-layer cages in the course of the dissolution of the solid  $\text{CaCO}_3$  core in the fluorescence microscope (Figure 16). After crosslinking the amino groups of the S-layer protein with glutaraldehyde the core was dissolved with EDTA. After this treatment the remaining structures looked smaller and more transparent.

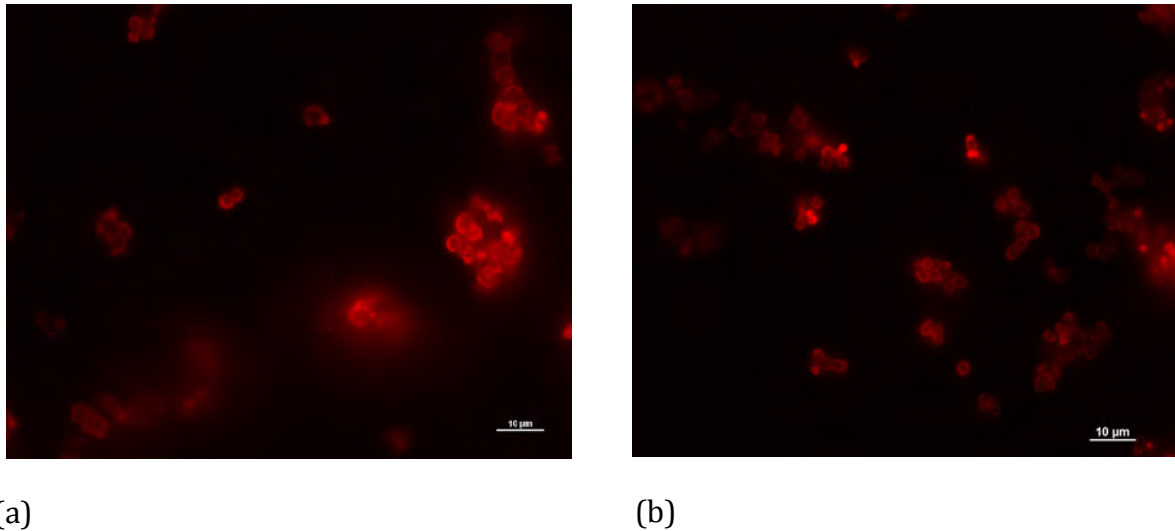


Fig.16  $\text{CaCO}_3$  particles coated with SgsE-mRFP fusion protein (and cross linked with glutaraldehyde) (a) before and (b) after EDTA-dissolution of the core.

In accordance to the work with S-layer coated liposomes the S-layer was silicified, and after dissolution of the core yielding mechanically stable constructs (Figure 17).

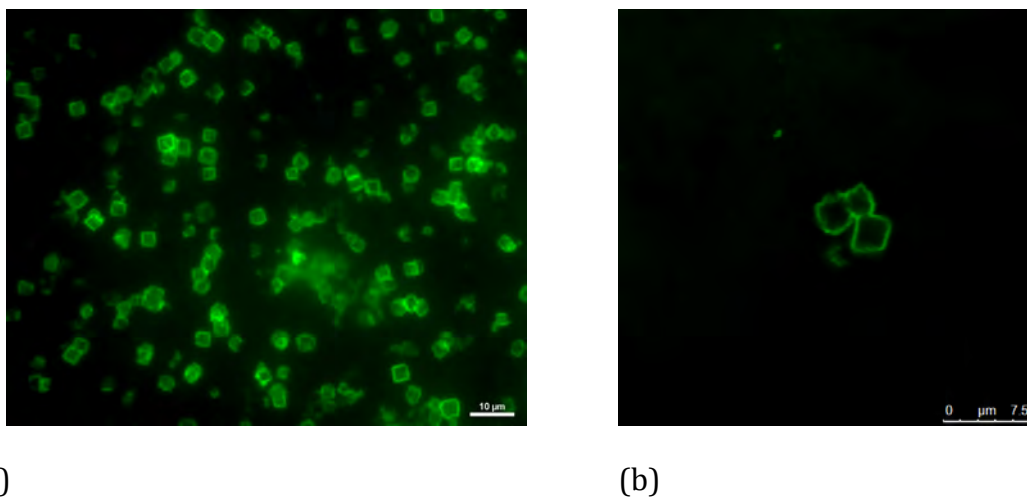


Fig.17 SgsE-EGFP coated silicified  $\text{CaCO}_3$ -particles after EDTA (0.2M) treatment. (a) conventional fluorescence microscopy, (b) confocal fluorescence microscopy

In an alternative approach, yellow fluorescence protein (YFP) was encapsulated into the core and its release through the S-layer coating (after dissolution of the solid calcium carbonate core) monitored in the fluorescence microscope (Figure 18). This experiment gave us the opportunity to watch the formation of S-layer cages without the need of using a fluorescent S-layer fusion protein.

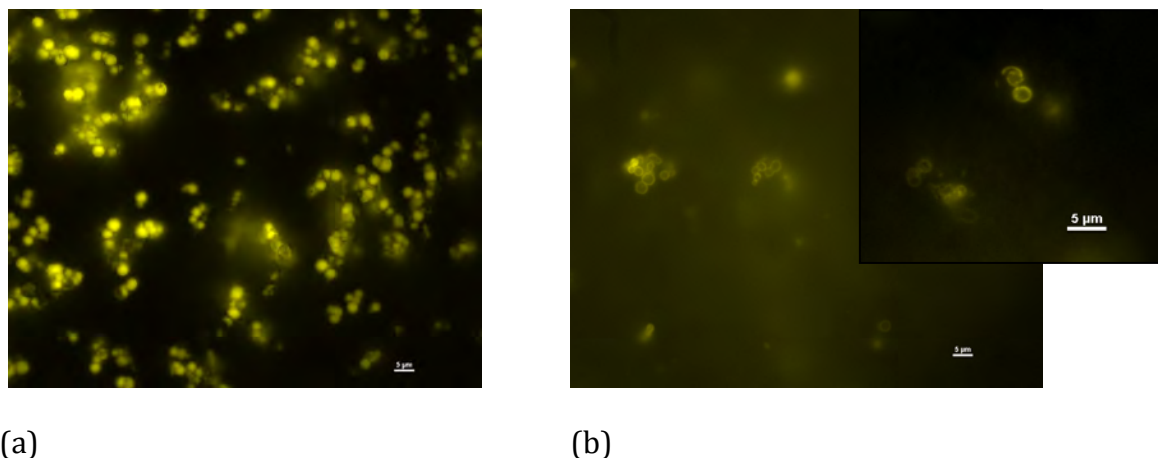


Fig.18  $\text{CaCO}_3$  particles, loaded with YFP, coated with SbpA and cross linked with Glutaraldehyde (a) before and (b) after EDTA-dissolution of the core.

In summary, this set of experiments demonstrated that the (crosslinked) S-layer coated cages remained intact after dissolution of the core.

### 5.3 S-layer coated nanocapsules

Although  $\text{CaCO}_3$  core were successfully coated with the SgsE-mRFP fusion protein, as described above, this part of the project was focused primarily on using nanocapsules made of alternatively charged polyelectrolyte layers enclosing the core as scaffolds.<sup>45</sup> Subsequently these nanocapsules were coated with an S-layer, silicified and the core removed by treatment with EDTA (Figure 19).

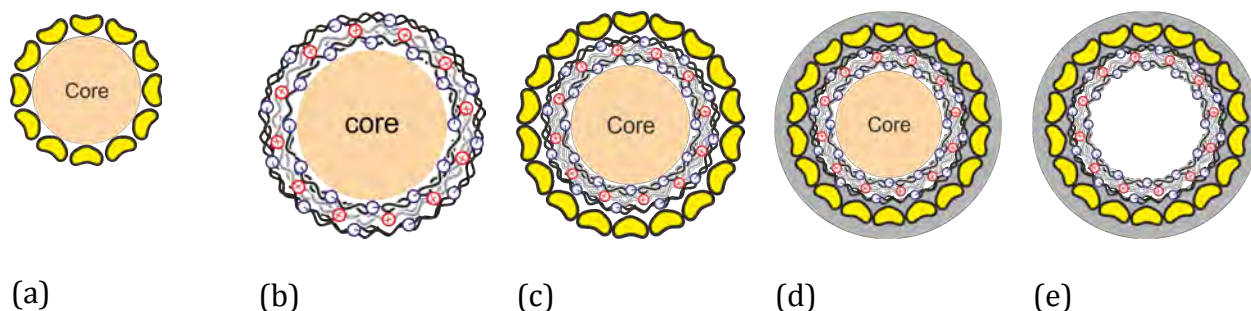


Fig.19 Schematic drawing of making S-layer coated silicified polyelectrolyte nanocapsules (a-d). As the final preparation step the core is dissolved leading to a closed rigid nanocontainer (e). In an alternative approach leading to the same results the core was already dissolved prior to step (c) or (d).

SbpA-PE<sub>x</sub>-capsules were fabricated according to the following procedure: In the first step CaCO<sub>3</sub> crystals were precipitated and coated with 2, 4 or 6 polyelectrolyte layers [(PAH<sup>+</sup>/PSS<sup>-</sup>)<sub>1-3</sub>; in 0.5M NaCl solution], starting with the positively charged PAH<sup>+</sup> (20min under rotation) and finishing with the negatively charged PSS<sup>-</sup>. Subsequently, two different routes were investigated: In one case (i) the CaCO<sub>3</sub>-Polyelectrolyte crystals were coated with SbpA (over night, 0.5mM Tris/HCl pH 9 10mM CaCl<sub>2</sub>) before resolving the CaCO<sub>3</sub>-core with EDTA. In the other case (ii) the core was resolved with EDTA before coating the polyelectrolyte capsules with SbpA. The results of the two alternative preparation routes were equivalent. The formation of CaCO<sub>3</sub>-crystals, the polyelectrolyte layer assembly, the S-layer coating and the results of the core dissolution were controlled by light, scanning electron (SEM) and scanning force (AFM) microscopy (Figure 20).

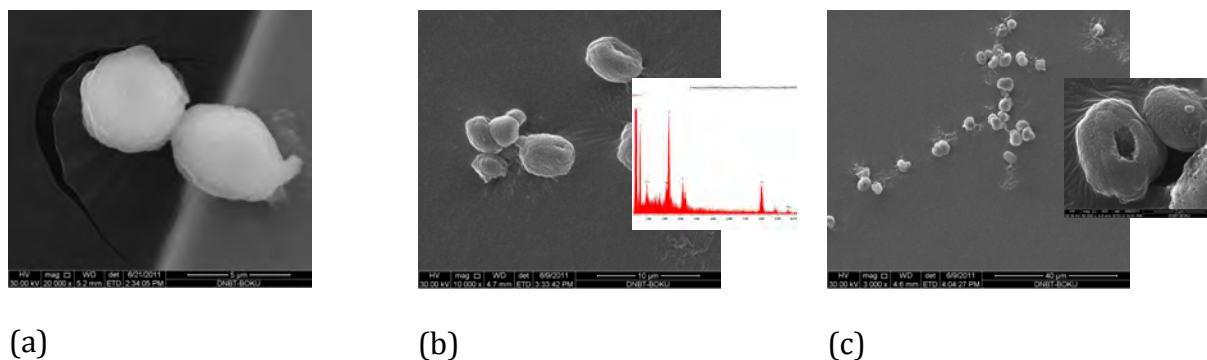


Fig.20 (a) SEM image of a CaCO<sub>3</sub> core encapsulated by PE<sub>4</sub>. (b) SEM image of a polyelectrolyte shell PE<sub>4</sub> without core. No calcium could be detected by EDX (inset) anticipating a complete dissolution of the core. (c) SEM of S-layer coated silicified polyelectrolyte (PE<sub>6</sub>) shells. The inset shows a zoomed view. An open nanocapsule is shown since it allows to have a look at the layer thickness of the polyelectrolyte shell and the empty interior. The S-Layer is not visible in the SEM image.

AFM measurements were carried out with SbpA-PE<sub>6</sub>-capsules adsorped on a PEI<sup>+</sup> coated glass slides. Contact mode was used to resolve the square (p4) lattice structure of the SbpA-PE<sub>6</sub>-capsule surface (see Figure 21).

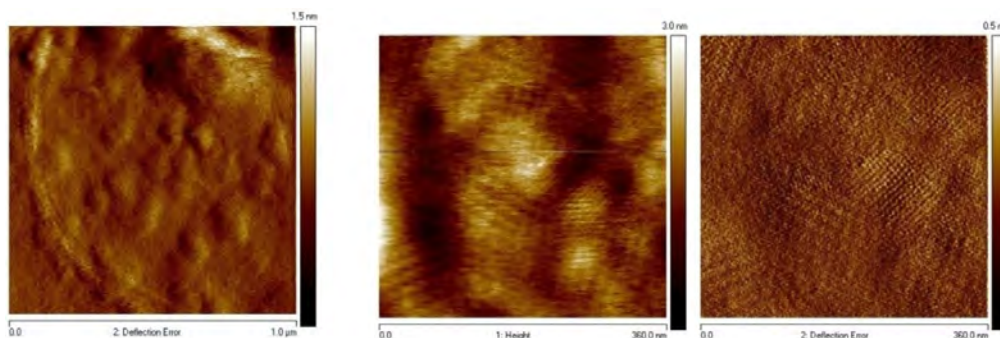


Fig.21 AFM images of SbpA coated polyelectrolyte capsules adsorped on a PEI coated glass slide. The left image shows an overview of the adsorped SbpA-PE<sub>6</sub>- capsule while in the middle and right image the p4 nanostructure is clearly visible.

In addition, TEM allowed visualizing the constructs, too (Figure 22).

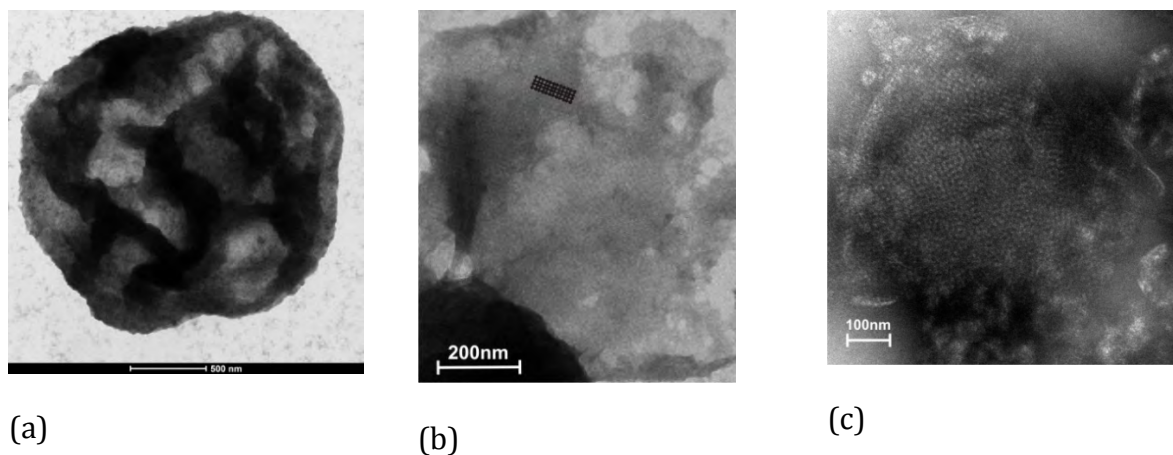


Fig.22 TEM images of SbpA coated polyelectrolytecapsules. (a) SbpA-PE<sub>4</sub>-capsule cross-linked with glutaraldehyde and stained with UA (1%, neutral NH<sub>3</sub>, 10min), (b) p4 lattice symmetry found on capsule-fragments, and (c) SbpA-PE<sub>6</sub>-capsule, cross-linked with glutaraldehyde and stained with UA. The p4 lattices are clearly visible.

## 5.4 Encapsulation of gold nanoparticles

Another idea demonstrating the successful making of hollow nanocapsules was to encapsulate gold nanoparticles and to silicify the SbpA-PE<sub>4</sub>-capsules. Therefore a gold nanoparticle solution (particle size 15-20 nm) was added to the precipitation reaction



when  $\text{CaCO}_3$ -crystals were formed. The  $\text{PE}_4$ -capsules with the encapsulated gold nanoparticles were coated with SbpA and silicified. The gold nanoparticle solution was very diluted that's the reason why only a few gold nanoparticles were found in the capsules as shown in the TEM image in Figure 23 (marked area). With EDX analysis silicon and gold were verified, see EDX spectrum in Figure 23c. However, it must be stressed here that gold nanoparticles were only found inside the shells (and not in the background) (Figure 23a). This result is important since it demonstrated that the constructs remained intact and the 15-20nm sized gold nanoparticles could not penetrate the 4-5nm pores in the S-layer.

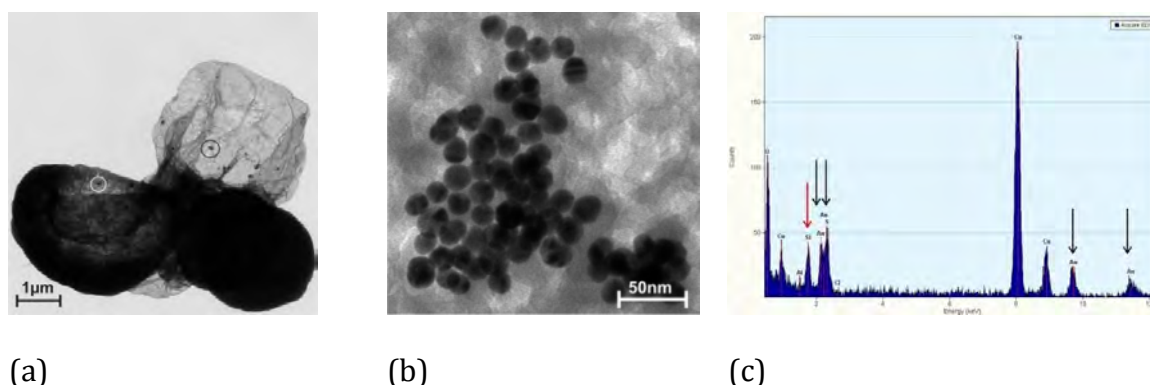


Fig.23 TEM investigations of silicified SbpA- $\text{PE}_4$ -capsules with encapsulated gold nanoparticles. (a) TEM image of three silicified SbpA- $\text{PE}_4$ -capsules with encapsulated gold nanoparticles. The Au-NP are located in the marked areas. (b) Encapsulated gold nanoparticles with a size between 15-20nm. (c) EDX spectrum of (a) indicating the silicon peak (red arrows) and the gold peaks (black arrows).

## 5.5 Conclusion – Nanocapsules

In summary, the making of hollow nano containers based on the coating of nanocapsules with S-layers and the subsequent silicification was successful. The complete dissolution of the core with EDTA (as determined by EDX analysis) gave stable silica supported S-layer architectures. In comparison, S-layer – PE composite coatings were more stable than plain S-layers. Furtheron, since gold nanoparticles immersed in the  $\text{CaCO}_3$  core were not released in the course of the dissolution of the core the integrity of the empty constructs could be demonstrated.

**Manuscript in preparation**

**Fabrication of robust hollow nanocapsules**

## 6 Lipid lamellae, foams and microbubbles

### 6.1 S-layer protein – lipid lamellae

The investigation of S-layer protein reassembly at bubble surfaces in wet aqueous foams for making (sub)micron sized “polyhedral cells” is closely related to the reassembly of S-layer proteins at liposomes and at planar lipid films. Since drainage is one of the dominating factors causing collapse of the foam (due to film rupture) we decided to start with the investigation of the most important parameters, such as the lipid-protein ratio, at foam lamellae. For this purpose a dedicated device, the so called Scheludko cell <sup>46</sup>, was used. A schematic drawing of this cell and its setup at an optical microscope is shown in Figure 24. The main part of the cell consists of a glass ring with holes at its inner diameter allowing to make a geometrically well defined film lamella (diameter and thickness) by a filling/sucking procedure. Film thicknesses, thinning over time and eventually the mechanical robustness were determined from the interference colors and intensities of light reflected from the front and back surfaces of the films.

As lipid Cetrimonium bromide ( $[(C_{16}H_{33})N(CH_3)_3Br]$ , cetyltrimethylammonium bromide, hexadecyltrimethylammonium bromide, CTAB) was used (Figure 25).

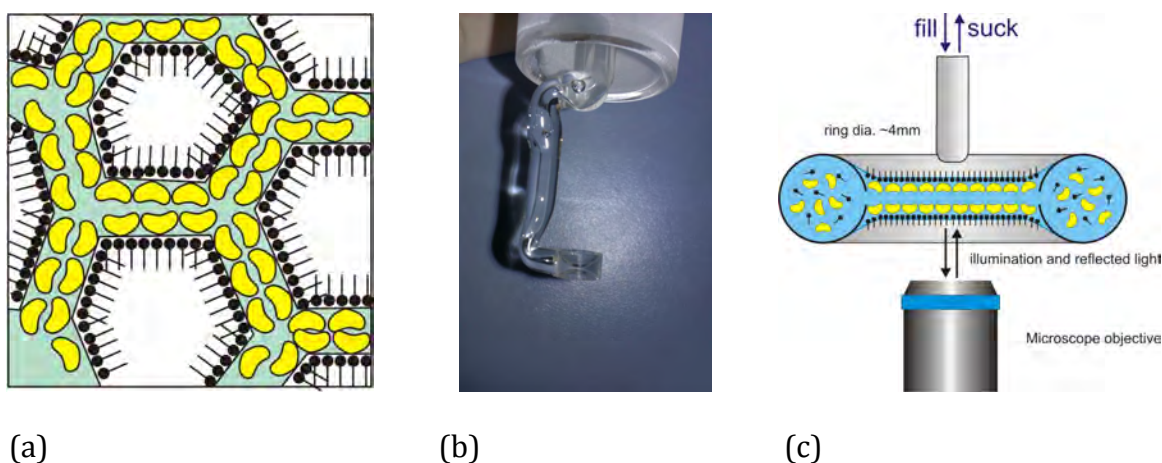


Fig.24 (a) Schematic drawing of S-layer coated foam bubbles, (b) glass ring (main part) and (c) schematic drawing of the Scheludko cell.

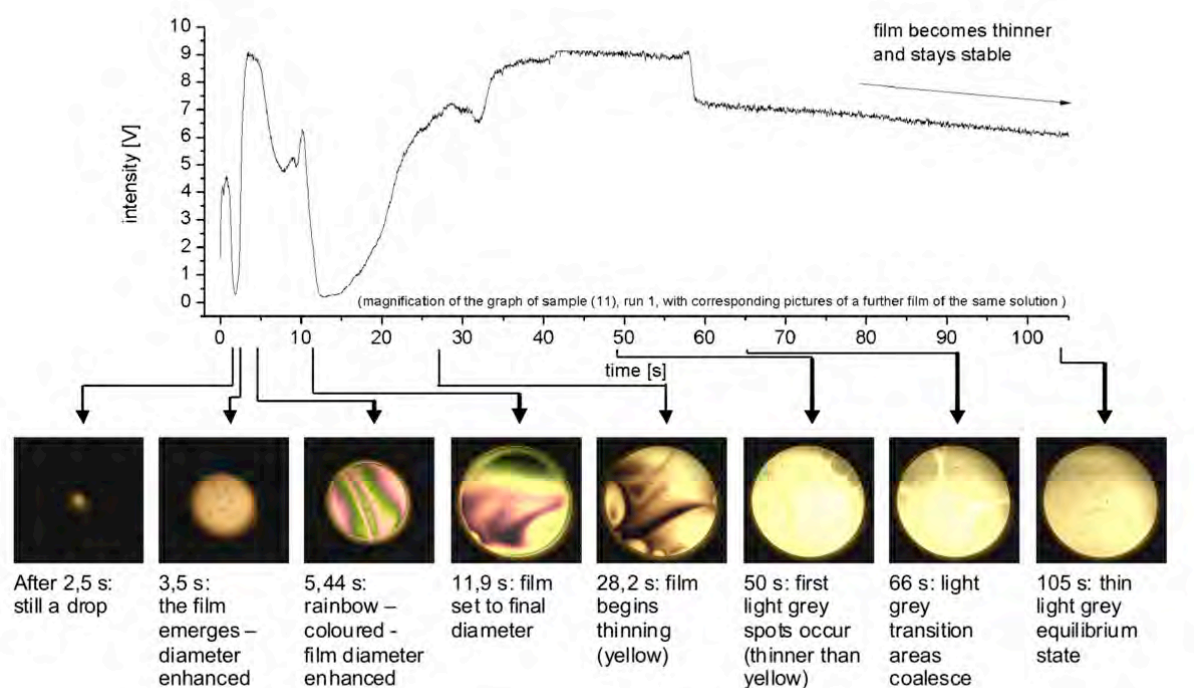


Fig.25 Interferometry images of **lipid (CTAB) 0,01 M** (after several minutes) showing the transition to a thinner state.

In the following experiments liquid film lamellae were generated from solutions of the S-layer protein SbpA and increasing lipid concentration (Figure 26 and 27). CTAB is dominant at the surface. SbpA proteins are displaced by CTAB from the film surface to the meniscus of the solution. The films were very stable, but behaved more or less like typical surfactant films without proteins.



Fig.26 Interferometry images of **SbpA 0.05 mg/ml in ~ 0.01 M CTAB**.



Some small coloured spots “swimming” on homogenous areas of different colours indicate protein aggregates (tagged by red arrows) which are finally displaced from the surface by CTAB (Figure 27).

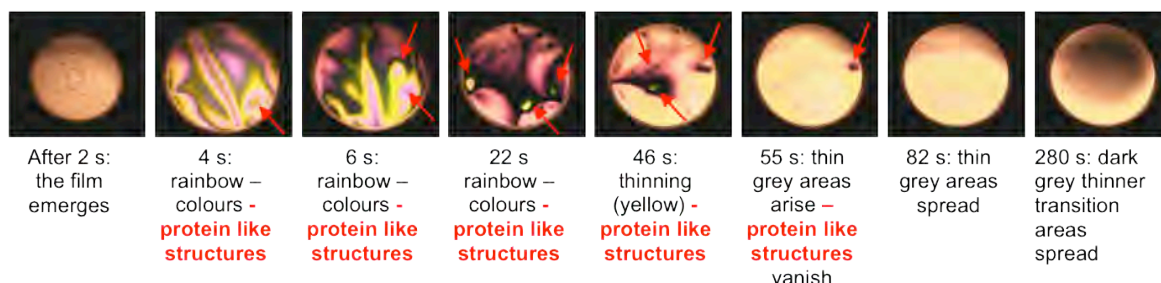


Fig. 27 Interferometry images of **SbpA 0,05 mg/ml** in  $\sim 10^{-5}$  M CTAB

In addition, the reassembly of S-layer protein at the air-water interface (without lipids) was studied, too (Figure 28). S-layer proteins without supporting lipids formed stable foam like lamellae. The film thinning showed that the air/water interface is rigid presenting a simple structure in the middle (analogous to other protein foam films). Protein foams were of higher thickness (compared to lipid supported foams) and did not reach equilibrated thin films. Since less surface movement was observed it was concluded that pure S-layer films provide less mechanical flexibility.

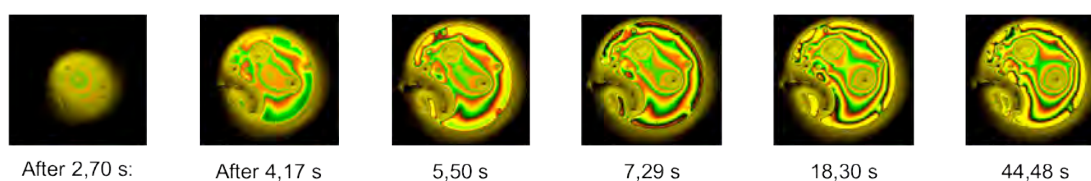


Fig.28 Interferometry images of **SbpA 0,05 mg/ml** in  $\sim 0,1$  M NaCl

## 6.2 Conclusions – lipid lamellae and foams

Stable, but rather thick films were obtained from SbpA in water. To achieve thinner films, while keeping the SbpA concentration as high as possible, the detergent CTAB as additional surfactants was added. From CTAB/SbpA mixtures very thin common- and Newton black

films were formed. However, their surface behavior was dominated by CTAB. However, three-dimensional foams are comprised of a network of interconnected thin liquid film lamellae. Hence, thin foam films are the building blocks affecting the stability of foams. Although the drainage and the disruption of foams, which are the much more complex system, is different from the respective events in isolated horizontal foam films, the investigation of single foam film lamellae have delivered promising results for the understanding of the stability of composite S-layer foams.

### **Master thesis**

Michael Schödelbauer. Biophysical properties of S-layer protein / surfactant foam lamellae and monolayers. Universität für Bodenkultur Wien (2012)

### **Manuscript in preparation**

Biophysical properties of S-layer protein / surfactant foam lamellae and monolayers  
Pum, D., Schödelbauer, M., Sleytr, U.B., Toca-Herrera, J. L.

## **6.3 S-layer coated microbubbles**

Based on standard procedures for the reassembly of S-layer proteins on liposomes and at the air-water interface, particular protocols for coating and handling micrometer sized gas filled micro bubbles were developed. Such micro spheres have been in use for ultrasonic echography in medical diagnostics. Dipalmitoylphosphatidylglycine ( DPPG ) and Dipalmitoylphosphatidylcholin ( DPPC ) in a ratio of 1:4 were used as natural biological detergents for making the spherical structures based on the hydrophobic effect. Since air will diffuse out of the bubbles too quickly it was replaced by sulfur hexafluoride (SF<sub>6</sub>) gas (Figure 29).

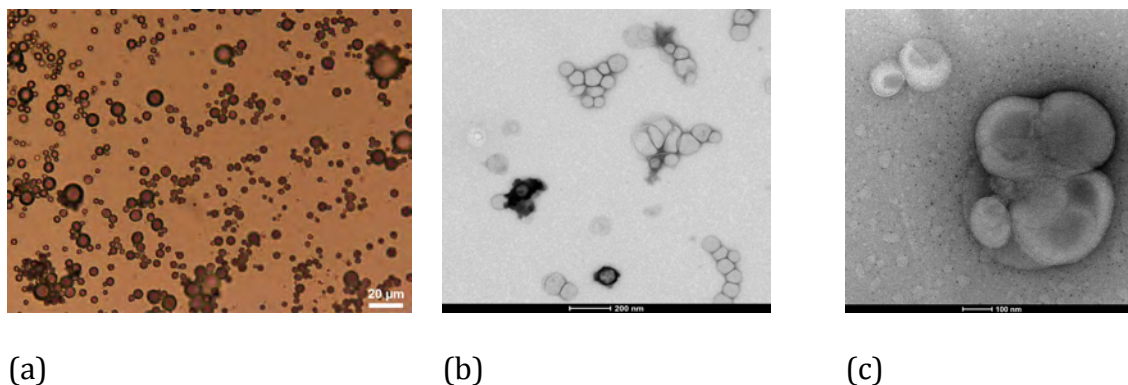


Fig.29 (a) Light microscopic image of lipid+SbpA mechanically bubbled with SF<sub>6</sub>. (b) and (c) TEM images of negatively stained preparations of DPPC-Cholesterol-HDA+SbpA+SF<sub>6</sub>+glutaraldehyde cross-linked micro bubbles.

It was found that the S-layer coating with SbpA had a stabilizing effect on the micro bubbles increasing the life time up to 2 hours. Nevertheless, in the course of the reassembly of the S-layer proteins the bubbles aggregated and thus did not allow to obtain “pure” S-layer cages. Work in progress.

## 7 Cylindrical S-layer morphologies (tubes)

A further goal of this project concerned the formation of S-layer tubes. Previous experiments have demonstrated that optical glass and chalcogenide fibres may be coated with reassembled S-layer proteins. As a specific aim of this project we planned to reassemble S-layer protein on suitable fibers, crosslink the proteins, and to dissolve the fiber in a final step. The reassembly of S-layer proteins is established but the dissolution of the fibre without destroying the S-layer almost impossible. Thus it was decided to use multi walled carbon nanotubes as scaffolds instead. Preliminary results are promising and work will continue.

## 8 Design and expression of fluorescent S-layer fusion proteins and their spectroscopic characterization

The design and expression of fluorescent S-layer fusion proteins was an important contribution to the development of a molecular construction kit and, in particular, to the success of this project since it allowed to control the preparation of S-layer cages in their natural environments by fluorescence microscopy. Part of the work was funded by this grant and thus only the abstracts of the published work are reproduced here. The support of AFOSR is gratefully acknowledged in the publications.

### 8.1 Absorption, steady-state fluorescence, fluorescence lifetime and 2D self-assembly properties of engineered fluorescent S-Layer fusion proteins of *Geobacillus stearothermophilus* NRS 2004/3a.

Kainz, B., Steiner, K., Möller, M., Pum, D., Schäffer, C., Sleytr, U.B., Toca-Herrera, J.L., *Biomacromolecules*, 11 (2010) 207-214

S-layer fusion protein technology was used to design four different fluorescent fusion proteins with three different GFP mutants and the red fluorescent protein mRFP1. Their absorption spectra, steady-state fluorescence, and fluorescence lifetime were investigated as a function of pH. It was found that fluorescence intensities and lifetime of the GFP mutant S-layer fusion proteins decreased about 50% between pH 6 and pH 5. The spectral properties of the red S-layer fusion protein were minimally affected by pH variations. These results were compared with His-tagged reference fluorescent proteins, demonstrating that the S-layer protein did not change the general spectral properties of the whole fusion protein. In addition, the  $pK_a$  values of the fluorescent S-layer fusion proteins were calculated. Finally, it was shown that the S-layer fusion proteins were able to self-assemble forming 2D nanostructures of oblique p2 symmetry with lattice parameters of about  $a = 11$  nm,  $b = 14$  nm, and  $\gamma = 80^\circ$ . The fluorescence tag did not hinder the natural self-assembly process of the S-layer protein. The combination of the

fluorescence properties and the self-assembly ability of the engineered fusion proteins make them a promising tool to generate biomimetic surfaces for future applications in nanobiotechnology at a wide range of pH.

## 8.2 Fluorescent S-Layer Protein Colloids

Kainz, B., Steiner, K., Sleytr, U.B., Pum, D., Toca-Herrera, J. L., *Soft Matter* 6 (2010) 3809-3814

Four different coloured pH dependent biocolloids have been designed with fluorescent S-layer fusion proteins. The intrinsic self assembling capability of the S-layer protein SgsE on silicon dioxide particles lead to crystalline p2 lattice symmetry which was combined with the fluorescent properties of fused cyan ECFP, green EGFP, yellow YFP and red mRFP1. Confocal microscopy was used to monitor the pH dependence of the fluorescent S-layer coating. Electrophoretic measurements were carried out to understand the colloidal behaviour of the S-layer protein coated particles. It was found with flow cytometry that the stable SgsE-ECFP, SgsE-EGFP, SgsE-YFP and SgsE-mRFP bioparticle suspensions lost 50% of their fluorescence emission at the  $pK_a$  of the chromophores. These novel fluorescent S-layer biocolloids can be used as pH sensors and might have an important role in surface pH determination.

## 8.3 Fluorescent energy transfer in the bi-fluorescent S-layer tandem fusionprotein ECFP-SgsE-YFP

Kainz, B., Steiner, K., Sleytr, U.B., Pum, D., Toca-Herrera, J. L., *J. Struct. Biol.* 172 (2010) 276-283

This work reports for the first time on the fabrication of a bi-functional S-layer tandem fusion protein which is able to self-assemble on solid supports without losing its functionality. Two variants of the green fluorescent protein (GFP) were genetically combined with a self-assembly system having the remarkable opportunity to interact with each other and act as functional nanopatterning biocoating. The S-layer protein SgsE of *Geobacillus stearothermophilus* NRS 2004/3a was fused with the cyan ECFP donor protein

at the SgsE N-terminus and with the yellow YFP acceptor protein at the C-terminus. The fluorescence energy transfer was studied with spectrofluorimetry, confocal microscopy and flow cytometry, whilst protein self-assembly (on silicon dioxide particles) and structural investigations were carried out with atomic force microscopy (AFM). The fluorescence resonance energy transfer efficiency of reassembled SgsE tandem protein was  $20.0 \pm 6.1\%$  which is almost the same transfer efficiency shown in solution ( $19.6 \pm 0.1\%$ ). This work shows that bi-fluorescent S-layer fusion proteins self-assemble on silica particles retaining their fluorescent properties.

## 9 Investigation of S-layer protein reassembly by electrochemical methods

In close collaboration with Prof. Wolfgang Kautek, Institute of Physical Chemistry at the University of Vienna the reassembly of S-layer proteins was investigated by electrochemical methods and by FTIR. Part of this work was funded by this grant and thus only the abstracts are included here. The support of AFOSR is gratefully acknowledged in the publications.

### 9.1 Electrochemical control of adsorption dynamics of surface layer proteins on gold

Zafiu, C., Trettenhahn, G., Pum, D., Sleytr, U.B., Kautek, W., Phys. Chem. Chem. Phys. 13 (2011) 3478-3483

The kinetics and mechanism of the adsorption of the surface layer proteins of *Lysinibacillus sphaericus* CCM2177 on gold depend on the charging conditions of the electrochemical double layer and the addition of  $\text{Ca}^{2+}$  ions. The electrical and mass charging was monitored by an in situ electrochemical quartz microbalance. Adsorption and monolayer formation of the protein molecules occur in the positive potential region where solvated anions form the electrochemical double layer. The crystalline character of the surface layer was diagnosed by an atomic force microscope. Negative of the point of zero charge, multilayer island structures were found.

## 9.2 Structural Control of Surface Layer Proteins at Electrified Interfaces investigated by In Situ Fourier Transform Infrared Spectroscopy

Zafiu, C., Trettenhahn, G., Pum, D., Sleytr, U.B., Kautek, W. , Phys. Chem. Chem. Phys. 13 (2011) 13232-13237

In situ Fourier Transform Infrared (FTIR) Spectroscopy complemented by Electrochemical Quartz Microbalance (EQMB) investigations allowed a detailed insight into the influence of the electrode potential on competing adsorption processes and bonding mechanisms of buffer ions and S-layer protein molecules of *Lysinibacillus sphaericus* CCM2177 at an electrified liquid/gold interface. The S-layer proteins adsorb on gold polarized positively of the point of zero charge by displacing perchlorate anions in the Helmholtz plane by their carboxylate groups. This is indicated by an increase of the peptide and carboxylate infrared absorption signals accompanied by a decrease of the perchlorate signal. S-layers interlinked laterally with  $\text{Ca}^{2+}$  ions, positive of the point of zero charge, resulted in the formation of a crystalline layer participating in the Helmholtz layer. In contrast to the absence of the  $\text{Ca}^{2+}$ -linkers, S-layers remain structurally intact also in the negative polarization domain where the Helmholtz layer is solely sustained by mainly solvated cations without participation of the negatively charged protein carboxylate functions.

## 10 Molecular dynamic and Monte Carlo simulations of S-layer protein reassembly

The experimental work was assisted by calculating 3D-structure predictions of the used S-layer proteins. The self-assembly process was investigated by Monte-Carlo simulations. All results are published already and hence only the abstracts are reproduced here. The support of AFOSR is gratefully acknowledged in the publications.

**Note:** This work was performed in close collaboration with Prof. M. Muthukumar, University of Massachusetts, Amherst, MA (USA).

### **10.1 Surface layer protein characterization by small angle x-ray scattering and a fractal mean force concept: From protein structure to nano-disc assemblies**

Horejs, C., Pum, D., Sleytr, U.B., Peterlik, H., Jungbauer, A., Tscheliessnig, R., J. Chem. Phys. 133 (2010) 175102-1-8

Surface layers (S-layers) are the most commonly observed cell surface structure of prokaryotic organisms. They are made up of proteins that spontaneously self-assemble into functional crystalline lattices in solution, on various solid surfaces, and interfaces. While classical experimental techniques failed to recover a complete structural model of an unmodified S-layer protein, small angle x-ray scattering (SAXS) provides an opportunity to study the structure of S-layer monomers in solution and of self-assembled two-dimensional sheets. For the protein under investigation we recently suggested an atomistic structural model by the use of molecular dynamics simulations. This structural model is now refined on the basis of SAXS data together with a fractal assembly approach. Here we show that a nondiluted critical system of proteins, which crystallize into monomolecular structures, might be analyzed by SAXS if protein-protein interactions are taken into account by relating a fractal local density distribution to a fractal local mean potential, which has to fulfill the Poisson equation. The present work demonstrates an important step into the elucidation of the structure of S-layers and offers a tool to analyze the structure of self-assembling systems in solution by means of SAXS and computer simulations.

### **10.2 Monte Carlo study of the molecular mechanisms of S-layer protein self-assembly**

Horejs, C., Mitra, M. K., Pum, D., Sleytr, U.B., Muthukumar, M., J. Chem. Phys. 134 (2011) 125103-1-11

The molecular mechanisms guiding the self-assembly of proteins into functional or pathogenic largescale structures can be only understood by studying the correlation between the structural details of the monomer and the eventual mesoscopic morphologies. Among the myriad structural details of protein monomers and their manifestations in the



self-assembled morphologies, we seek to identify the most crucial set of structural features necessary for the spontaneous selection of desired morphologies. Using a combination of the structural information and a Monte Carlo method with a coarse-grained model, we have studied the functional protein self-assembly into S(surface)-layers, which constitute the crystallized outer most cell envelope of a great variety of bacterial cells. We discover that only few and mainly hydrophobic amino acids, located on the surface of the monomer, are responsible for the formation of a highly ordered anisotropic protein lattice. The coarse-grained model presented here reproduces accurately many experimentally observed features including the pore formation, chemical description of the pore structure, location of specific amino acid residues at the protein–protein interfaces, and surface accessibility of specific amino acid residues. In addition to elucidating the molecular mechanisms and explaining experimental findings in the S-layer assembly, the present work offers a tool, which is chemical enough to capture details of primary sequences and coarse-grained enough to explore morphological structures with thousands of protein monomers, to promulgate design rules for spontaneous formation of specific protein assemblies.

Note: This work was performed in close collaboration with Prof. M. Muthukumar, Univ. of Massachusetts, USA.

### **10.3 Atomistic structure of monomolecular surface layer self-assemblies: towards functionalized nanostructures**

Horejs, C., Gollner, H., Pum, D., Sleytr, U.B., Peterlik, H., Jungbauer, A., Tschliessnig, R., ACS Nano 5 (2011) 2288-2297

The concept of self-assembly is one of the most promising strategies for the creation of defined nanostructures and therefore became an essential part of nanotechnology for the controlled bottom-up design of nanoscale structures. Surface layers (S-layers), which represent the cell envelope of a great variety of prokaryotic cells, show outstanding self-assembly features in vitro and have been successfully used as the basic matrix for molecular construction kits. Here we present the three-dimensional structure of an S-layer lattice

based on tetrameric unit cells, which will help to facilitate the directed binding of various molecules on the S-layer lattice, thereby creating functional nanoarrays for applications in nanobiotechnology. Our work demonstrates the successful combination of computer simulations, electron microscopy (TEM), and small-angle X-ray scattering (SAXS) as a tool for the investigation of the structure of self-assembling or aggregating proteins, which cannot be determined by X-ray crystallography. To the best of our knowledge, this is the first structural model at an amino acid level of an S-layer unit cell that exhibits p4 lattice symmetry.

## 11 Single molecule force spectroscopy

In addition to the theoretical work on S-layer proteins a most remarkable result was obtained by single molecule force spectroscopy. It was found that the interaction of the S-layer protein with the secondary cell wall polymer of the associated bacterial cell wall increases the strength of the S-layer protein. This part of the work is published already, too, and thus only the abstract of the paper is reproduced here.

### 11.1 Single-molecule force spectroscopy reveals the individual mechanical unfolding pathways of a surface layer protein

Horejs, C., Ristl, R., Tscheliessnig, R., Sleytr, U.B., Pum, D., J. Biol. Chem. 286 (2011) 27416-27424

Surface layers (S-layers) represent an almost universal feature of archaeal cell envelopes and are probably the most abundant bacterial cell proteins. S-layers are monomolecular crystalline structures of single protein or glycoprotein monomers that completely cover the cell surface during all stages of the cell growth cycle, thereby performing their intrinsic function under a constant intra- and intermolecular mechanical stress. In Gram-positive bacteria, the individual S-layer proteins are anchored by a specific binding mechanism to polysaccharides (secondary cell wall polymers) that are linked to the underlying peptidoglycan layer. In this work, atomic force microscopy based single-molecule force spectroscopy and a polyprotein approach are used to study the individual mechanical

unfolding pathways of an S-layer protein. We uncover complex unfolding pathways involving the consecutive unfolding of structural intermediates, where a mechanical stability of 87 pN is revealed. Different initial extensibilities allow the hypothesis that S-layer proteins adapt highly stable, mechanically resilient conformations that are not extensible under the presence of a pulling force. Interestingly, a change of the unfolding pathway is observed when individual S-layer proteins interact with secondary cell wall polymers, which is a direct signature of a conformational change induced by the ligand. Moreover, the mechanical stability increases up to 110 pN. This work demonstrates that single-molecule force spectroscopy offers a powerful tool to detect subtle changes in the structure of an individual protein upon binding of a ligand and constitutes the first conformational study of surface layer proteins at the single-molecule level.

## 12 Conclusions from the project – Impact on the field

The development of an enabling technology for 3D-protein architectures based on self-assembly of native and/or genetically engineered bacterial S-layer proteins was completely new in biomaterial research and was established in the course of the project. S-layer self-assemblies offer the advantage of generating entirely new containers when used as catalysts, templates or scaffolds. In comparison to virus capsids (typically 30 to 100nm in diameter) or hollow (apo)ferritin (12 nm in diameter) S-layer vesicles may be much larger and adjustable in size.

Thus, several approaches differing in the respective sizes of the final nano constructs were developed ranging from the use of liposomes, over nanocapsules to microbubbles. The common building principle of the layered architectures comprised the coating with S-layer proteins serving as active layer in the formation of a well defined biogenic silica shell. This silica shell endowed the whole construct with mechanical robustness. Dissolution of the core material (lipids, calcium carbonate) led to the desired hollow nano containers. Basic research on S-layer supported lipid film lamella yielded an important contribution to the reassembly of S-layer proteins at the bubble surfaces in foams. The experimental work was supported by calculating 3D-structure predictions of the used S-layer proteins, by investigating the self-assembly process by Monte-Carlo simulations, and by fundamental

work on the strength of S-layer proteins. Part of the work was carried out in close collaboration with partners from other AFOSR-funded projects (C.C. Perry, Nottingham Trent University, Nottingham, UK and M. Muthukumar, Univ. of Massachusetts, MA).

We would like to anticipate a broad range of novel applications for S-layer protein cages ranging from the development of artificial viruses to templates for the synthesis of nanoparticles. The possibility to use native and recombinantly produced S-layer fusion proteins with incorporated functionalities opens a new horizon for material (e.g. drug) encapsulation, targeting and delivery. When using S-layer fusion proteins with catalytic sites exposed at the inner or outer face of the cages, a highly efficient templated biomineralization of metallic, semiconducting or other inorganic nanomaterials will be facilitated. Furthermore, S-layers offer a rich structural diversity in spacings and lattice types. The two-dimensional lattice parameters can vary from species to species, allowing one to “tune” the desired lattice constant and consequently the pore size for a particular application. Thus a variety of S-layer meshworks differing in their geometrical and physicochemical parameters will become available.

Up to now 11 SCI-cited papers from this work have been published already, several more are in preparation or submitted and two PhD thesis and one Master thesis were funded by this project.

We would like to thank the Air Force Office for Scientific Research (AFOSR) for funding this project !

## 13 References

1. Kröger, N., Lorenz, S., Brunner, E., Sumper, M. *Science* **2002**, 298, 584-6.
2. Cha, J. N., Shimizu, K., Zhou, Y., Christiansen, S. C., Chmelka, B. F., Stucky, G. D., Morse, D. E. *Proc. Natl. Acad. Sci. U. S. A.* **1999**, 96, 361-5.
3. Zlotnick, A. *J. Mol. Biol.* **1994**, 241, 59-67.
4. Horne, R. W., Wildy, P. *Virology* **1961**, 15, 348-373.
5. Chasteen, N. D., Harrison, P. M. *J. Struct. Biol.* **1999**, 126, 182-94.
6. Lambert, E. M., Viravaidya, C., Li, M., Mann, S. *Angew. Chem., Intl. Ed.* **2010**, 49, 4100-3.

7. Sleytr, U.B., Messner, P., Pum, D., Sára, M. *Angew. Chem., Intl. Ed.* **1999**, 38, 1034-1054.
8. Sleytr, U.B., Huber, C., Ilk, N., Pum, D., Schuster, B., Egelseer, E. M. *FEMS Microbiol. Lett.* **2007**, 267, 131-144.
9. Sleytr, U.B., Egelseer, E. M., Ilk, N., Pum, D., Schuster, B. *FEBS J.* **2007**, 274, 323-334.
10. Sára, M., Sleytr, U.B. *J. Bacteriol.* **1987**, 169, 4092-4098.
11. Messner, P., Pum, D., Sára, M., K. O. Stetter, Sleytr, U.B. *J. Bacteriol.* **1986**, 166, 1046-1054.
12. Pum, D., Messner, P., Sleytr, U.B. *J. Bacteriol.* **1991**, 173, 6865-6873.
13. Sleytr, U.B. *Int. Rev. Cytol.* **1978**, 53, 1-64.
14. Pum, D., Sleytr, U.B. *Supramolec. Sci.* **1995**, 2, 193-197.
15. Györvary, E.S., Stein, O., Pum, D., Sleytr, U.B. *J. Microscopy* **2003**, 212, 300-306.
16. Pum, D., Weinhandl, M., Hödl, C., Sleytr, U.B. *J. Bacteriol.* 1993, 175, 2762-2766.
17. Pum, D., Sleytr, U.B. *Thin Solid Films* **1994**, 244, 882-886.
18. Schuster, B., Sleytr, U.B. *Rev. Mol. Biotechnol.* **2000**, 74, 233-254.
19. Küpcü, S., Sára, M., Sleytr, U.B. *Biochim. Biophys. Acta* **1995**, 1235, 263-269.
20. Mader, C., Küpcü, S., Sára, M., Sleytr, U.B. *Biochim. Biophys. Acta* **1999**, 1418, 106-116.
21. Mader, C., Küpcü, S., Sleytr, U.B., Sára, M. *Biochim. Biophys. Acta* **2000**, 1463, 142-150.
22. Toca-Herrera, J.L., Krastev, R., Bosio, V., Küpcü, S., Pum, D., Fery, A., Sára, M., Sleytr, U.B. *Small* **2005**, 3, 339-348.
23. Delcea, M., Krastev, R., Gutlebert, Th., Pum, D., Sleytr U.B., Toca-Herrera, J.L. *J. Nanosc. Nanotechn.* **2007**, 7, 4260-4266.
24. Delcea, M., Krastev, R., Gutberlet, T., Pum, D., Sleytr, U.B., Toca-Herrera, J. L. *Soft Matter* **2008**, 4, 1414-1421.
25. Göbel, C., Schuster, B., Baurecht, D., Sleytr, U., Pum, D. *Colloids Surf. B Biointerfaces* **2010**, 75, 565-72.
26. Horejs, C., Pum, D., Sleytr, U.B., Tscheliessnig, R. *J. Chem. Phys.* **2008**, 128, 65106-1-11
27. Horejs, C., Gollner, H., Pum, D., Sleytr, U.B., Peterlik, H., Jungbauer, A., Tschliessnig, R. *ACS Nano* **2011**, 5, 2288-2297
28. Horejs, C., Mitra, M. K., Pum, D., Sleytr, U. B., Muthukumar, M. *J. Chem. Phys.* **2011**, 134, 125103-1 – 125103-11
29. Horejs, C., Ristl, R., Tscheliessnig, R., Sleytr, U.B., Pum, D. *J. Biol. Chem.* **2011**, 286, 27416-27424
30. Sára, M. *Trends Microbiol.* **2001**, 9, 47-49.
31. Sára, M., Kuen, B., Mayer, H. F., Mandl, F., Schuster, K.C., Sleytr, U.B. *J. Bacteriol.* **1996**, 178, 2108-17.

32. Ilk, N., Völlenkle, C., Egelseer, E.M., Breitwieser, A., Sleytr, U.B., Sára, M. *Appl. Environ. Microbiol.* **2002**, 68, 3251-3260.
33. Messner, P., Pum, D., Sleytr, U.B. *J. Ultrastruct. Mol. Struct. Res.* **1986**, 97, 73-88.
34. Moll, D., Huber, C., Schlegel, B., Pum, D., Sleytr, U.B., Sára, M. *PNAS* **2002**, 99, 14646-14651.
35. Ilk, N., Egelseer, E.M., Pum, D., Schuster, B., Sleytr, U.B. *Colloids and Surfaces A: Physicochem. Eng. Aspects* **2007**, 321, 163-167.
36. Schäffer, C., Novotny, R., Küpcü, S., Zayni, S., Scheberl, A., Friedmann, J., Sleytr, U.B., Messner, P. *Small* **2007**, 3, 1549-1559.
37. Belton, D. J., Deschaume, O., Patwardhan, S. V., Perry, C. C. *J. Phys. Chem. B* **2010**, 114, 9947-9955.
38. Perry, C. C. *Prog. Mol. Subcell. Biol.* **2009**, 47, 295-313.
39. Perry, C. C., Belton, D., Shafran, K. *Prog. Mol. Subcell. Biol.* **2003**, 33, 269-99.
40. Chen, R. F., Knutson, J. R. *Anal. Biochem.* **1988**, 172, 61-77.
41. Hollmann, A., Delfederico, L., Glikmann, G., De Antoni, G., Semorile, L., Disalvo, E. A. *Biochim. Biophys. Acta, Biomembr.* **2007**, 1768, 393-400.
42. Sára, M., Sleytr, U.B. *J. Membr. Sci.* **1987**, 33, 27-49.
43. Sára, M., Pum, D., Sleytr, U.B. *J. Bacteriol.* **1992**, 174, 3487-93.
44. Sára, M., Küpcü, S., Weiner, C., Weigert, S., Sleytr, U.B. In *Immobilised Macromolecules: Application Potentials*, Sleytr, U.B., Messner, P., Pum, D., Sára, M., Eds., Springer-Verlag: London, UK, 1993, p 71.
45. Decher, G. *Science* **1997**, 277, 1232-1237
46. Scheludko, A. *Adv. Colloid Interface Sci.* **1967**, 1, 391-463.